Thesis
Subsidence mechanics of Kilauean pit cra
AC .H3 no.B81 15227
Blevins, James Y.
SOEST Library
HAWAII INSTITUTE OF GEOPHYSICS
LIBRARY ROOM

SUBSIDENCE MECHANICS OF KILAUEAN PIT CRATERS

A THESIS SUBMITTED TO THE GRADUATE DIVISION OF THE UNIVERSITY OF HAWAII IN PARTIAL FULFILLMENT OF THE REQUIREMENTS FOR THE DEGREE OF

MASTER OF SCIENCE

IN GEOLOGY AND GEOPHYSICS

by

James Y. K. Blevins Jr.

Thesis Committee:
Michael P. Ryan, Chairman
Eduard Berg
David Epp
Michael O. Garcia
George P. L. Walker

We certify that we have read this thesis and that in our opinion it is satisfactory in scope and quality as a thesis for the degree of Master of Science in Geology and Geophysics.

THESIS COMMITTEE

Chairman

ACKNOWLEDGEMENTS

The drafting skills of Marcia Prins and the photographic skills of Douglas Stalb are greatly appreciated. Critical reviews by David E. Epp, Michael O. Garcia and George P. L. Walker have been very helpful. The supply of unpublished deformation data and field equipment by the U. S. Geological Survey's Hawaiian Volcano Observatory is also appreciated. Discussions with Arnold T. Okamura of the Hawaiian Volcano Observatory regarding deformation of Kilauea and the development of Devil's Throat pit crater were of great value. Michael P. Ryan contributed countless hours to this project in the form of discussions, field assistance and reviews of this paper. Support by the U. S. Geological Survey's Geothermal Research Program under Grant No. 14-08-0001-G-631 to the University of Hawaii is gratefully appreciated.

ABSTRACT

The results of field observations and aerial photograph analyses of the pit craters on the upper east rift zone of Kilauea volcano, Hawaii, indicate that many pit craters have current boundaries defined by ENE oriented fractures, referred to here as bounding faults. The possibility of reconstructing a crater to it's initial formation size is suggested by transcurrent fissures. A detailed analyses of Devil's Throat crater is presented. A subsidence model, capable of recovering the three-dimensional geometry of a void at depth, is also presented. The model produces surface displacement fields similar to observed deformation patterns. Finally, the subsidence model is applied to each pit crater in the study area. The results indicate that craters near Kilauea's summit have initial collapse cavity depths nearer to the surface than do the craters further down the rift. The locations of the depths of the initial collapse cavities of the craters define a plane dipping 2.8^{o} to the southeast.

TABLE OF CONTENTS

ACKNOWLEDGEMENTS iii

ABSTRACT iv

LIST OF TABLES vi

LIST OF ILLUSTRATIONS vii

I. INTRODUCTION 1

II. THE PIT CRATERS 3

III. DEVIL'S THROAT 37

IV. SUBSIDENCE MECHANICS 52

V. SUBSIDENCE MECHANICS OF PIT CRATERS 66

VI. SUMMARY DISCUSSION 99

VII. CONCLUSIONS 101

APPENDIX AI 103

APPENDIX AII 106

BIBLIOGRAPHY 107

LIST OF TABLES

Table		Page
I	Devil's Throat crack analysis (I)	43
II	Devil's Throat crack analysis (II)	44
III	Devil's Throat section - flow unit thicknesses	48
IV	Devil's Throat section - intraflow joint spacing	49
V	Reconstructed pit crater diameters (I)	73
VI	Reconstructed pit crater diameters (II)	97

LIST OF ILLUSTRATIONS

Figure		Page
1	The summit caldera, southwest rift zone and upper east rift zone of Kilauea Volcano, Hawaii	5
2	Keanakakoi crater (aerial photograph)	12
3	Lua Manu crater and the neighboring eruptive vents of September, 1974	17
4	Puhimau crater	22
5	Hiiaka crater	27
6	The Pauahi complex	32
7	Devil's Throat	39
8	A sketch map of Devil's Throat showing the distribution of cracks around and near the crater	42
9	Devil's Throat section	46
10	A schematic representation of a three-dimensional rectilinear void of width 2a, length 2b and thickness t, buried at a depth, h	54
11	Normalized vertical displacement vs. normalized distance from the collapse cavity centerline	69
12	Crater diameter vs. the depth of the initial cavity nucleating the collapse sequence	71
13	Model deformation map of Keanakakoi crater	75
14	Model deformation map of Lua Manu crater	77
15	Model deformation map of Puhimau crater	79
16	Model deformation map of Kokoolau crater	81

17 Model deformation map of Devil's Throat crater 83

18 Model deformation map of Hiiaka crater 85

19 Model deformation map of Pauahi North crater 87

20 Model deformation map of Pauahi South crater 89

21 Model deformation map of Pauahi East crater 91

22 Sketch map of the Pauahi complex showing the relationship of the three craters' configurations when they initially formed 93

23 The relationship between the initial collapse cavity depth and a crater's cumulative distance from Halemaumau 95

24 Normalized subsidence curves corresponding to the the eruptive event of May 5, 1973 105

I. INTRODUCTION

Kilauea is a small shield volcano located on the southern portion of the island of Hawaii; the largest island in the Hawaiian chain. Kilauea rests on the south flank of Mauna Loa and is structurally characterized by a summit caldera and two rift zones; one trending in a gentle arc to the southwest and the other oriented approximately N70°E.

The east rift zone of Kilauea can be viewed as a combination of three segments. The upper east rift (Figure 1) extends from the summit caldera along a region of pit craters and eruptive fissures to Napau crater. The middle east rift begins at Napau crater and terminates near Puulena crater. There are no other pit craters between Napau and Puulena. The lower east rift is offset from the middle east rift, beginning roughly 1.5 km north of the terminus of the middle east rift and extending at least 20 km eastward across land and beneath the sea.

The upper east rift is an area with large lava fields, numerous fractures and eruptive fissures and three topographic highs: Puu Huluhulu, Kane Nui o Hama and Mauna Ulu. The most prominent features on the upper east rift are a collection of pit craters.

This study combines field observations of the structural setting and geometric nature of pit craters with the analytic subsidence mechanics of pit crater formation. The approach describes the initiation of pit crater formation as well as the controls on crater development and enlargement.

Throughout this study the term "pit crater" is applied only to roughly circular collapse features of various sizes whose origins are

not directly related to the drainage of a lava lake. This, then, excludes craters such as those atop cones and shields (i.e., Mauana Ulu's summit crater (Swanson and others, 1979)) and Halemaumau (Jaeggar, 1947).

It is hoped that this work will provide a basis for understanding the mechanics of pit crater formation, since pit craters are one of the key surface features which reflect subsurface structural conditions in a shield volcano.

II. THE PIT CRATERS

The study area extends from the southern margin of Kilauea's summit caldera, east for 8 km along the east rift zone. Craters included in the study have been Keanakakoi, Lua Manu, Puhimau, Kokoolau, Devil's Throat, Hiiaka and the craters of the Pauahi complex. Inaccessibility has prevented the field study of Aloi and Alae craters (due to burial by Mauna Ulu lava) and Makaopuhi. Figure 1 provides locations for the craters in the study area.

Throughout the following pit crater descriptions references are made to the nature of the vegetation in and around the craters, and may be used as indicators of preferential mass wastage and crater development.

COMMON PIT CRATER CHARACTERISTICS

The pit craters of the upper east rift zone have many common characteristics. For example, Brigham (1909) recorded that when the "pit craters of Puna" were first discovered by non-natives, the craters were thickly vegetated: the ancient floors of Makaopuhi, Alae and Kilauea Iki, contained forests of ohia trees. These observations indicate that the upper east rift may have been "quiet" for a considerable period. Also, there are presently two craters on the upper east rift zone which are a combination of at least two discrete craters: Makaopuhi and Pauahi. Such combinations of two individuals can be termed as double-craters. Before the Mauna Ulu eruption, Alae was also

Figure 1. The summit caldera, southwest rift zone and upper east rift zone of Kilauea volcano, Hawaii.

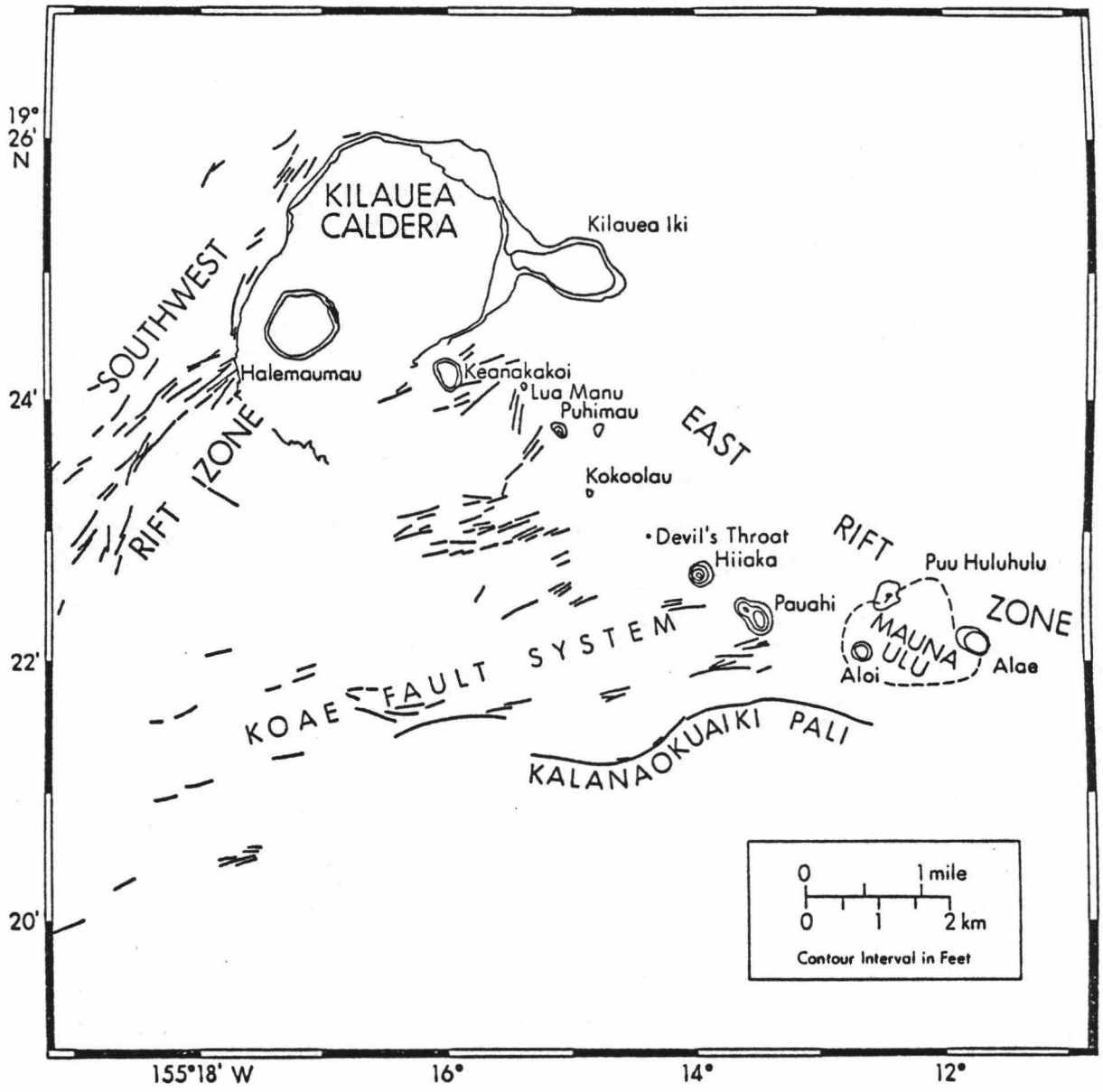
19° 26' N
24'
22'
20'
155°18' W
16°
14°
12°
KILAUEA CALDERA
Kilauea Iki
SOUTHWEST RIFT ZONE
Halemaumau
Keanakakoi
Lua Manu
Puhimau
EAST RIFT ZONE
Kokoolau
Devil's Throat
Hiiaka
Pauahi
Puu Huluhulu
MAUNA ULU
Aloi
Alae
KOAE FAULT SYSTEM
KALANAOKUAIKI PALI
0 1 mile
0 1 2 km
Contour Interval in Feet

a double crater. An interesting feature common to these three craters is that in each area the individual pits fall on a line which, when extended, points to Kilauea's summit.

Each crater in the study area has conspicuous faults tangent to it's southeast end. In many cases tangential faults on the NW margin are observed parallel to those on the SE. Most of these faults have strikes ranging from N60°E to N70°E. Closer to the summit area, the strikes change to N85°E and east-west. These major tangential faults are referred to here as "bounding faults".

The complex of craters that forms Pauahi has been divided into three areas, referred to as Pauahi North, Pauahi South and Pauahi East. Clearly, the complex is dominated by Pauahi North, the northern pit, and Pauahi South, the southern pit. To the east of Pauahi South is a small, shallow crater: Pauahi East.

GEOMETRIC NATURE OF THE PIT CRATERS

The physical dimensions of the pit craters on Kilauea's upper east rift zone are provided in the field observation section below, on a crater-by-crater basis. The lengths of the major and minor axes, both at the surface and on the floor of each crater, were obtained by measurements from airphotos and U. S. Geological Survey (7.5 min) topographic maps. Values were averaged if more than one source was used. The airphotos were taken by Air Survey Hawaii of Honolulu in December 1979. The scales have been corrected by measuring roadway medial stripes or parking lot stripes in the photographs, recovering the

true scaled measurements.

The depths of all craters, except for Devil's Throat and Puhimau, were derived from the topographic maps by taking the dimensions of the lava lake floors from the airphotos and, after changing scale, centering the lakes onto the topographic maps and counting the remaining contour lines. The depths for Devil's Throat and Puhimau crater were obtained by direct plumb line measurements.

Crater volumes were determined using formulae for:

(i) a cylinder with an elliptic base;
(ii) a cylinder with a circular base;
(iii) a frustum: a solid geometric figure with two circular bases of different radii

The area of an ellipse was taken as:

$$A = \pi ab \qquad (1)$$

where a and b are the lengths of the major and minor radii, respectively. Thus, the average area of the elliptic crater floor plus the elliptic crater surface has been multiplied by the crater depth to generate it's "elliptic" volume.

Circular volumes were determined by using the average of the mean surface diameter plus the mean floor diameter in the formula:

$$V = \pi h(d/2)^2, \qquad (2)$$

where h was the crater depth and d was the average crater diameter.

The volumes of craters were also derived using the formula for a frustum:

$$V = (1/3)\pi\, h(R_1R_2 + R_1^2 + R_2^2), \qquad (3)$$

where R_1 and R_2 were the average surface radius and average floor radius, respectively.

The volume for Puhimau crater, which has no level floor, was determined using the formula for a cone:

$$V = (1/3)\pi\, R_1^2 h\ . \qquad (4)$$

GEOMETRIC REGULARITIES

In addition to the specific geometric results, discussed below, two general relationships among craters have been determined. First, craters may be divided into two groups on the basis of the surface geometric aspect ratio. Group I, with an aspect ratio near 1.0, contains Kokoolau, Devil's Throat, Hiiaka, Pauahi North, Pauahi South and Pauahi East craters. Group II, with aspect ratios between 0.66 and 0.75, contains Keanakakoi, Lua Manu and Puhimau craters. Second, pit crater volumes fall into two categories. One group consists of large craters with volumes that are on the order of 10^6 m^3 and includes Keanakakoi, Puhimau, Hiiaka, Pauahi North and Pauahi South. The second group consists of Lua Manu and Devil's Throat, with volumes on the order of 10^4 m^3.

It is emphasized that a comparison between the present day pit crater morphology and the morphology which existed at the time the U. S. Geological Survey topographic maps were compiled (1963) shows that the volumes of pit craters and floor aspect ratios are temporal values. Surface aspect ratios and diameters, however, appear less likely to change with deformation and eruptive activity and may be regarded as an indicator of the collapse and mass wastage evolution of the individual crater.

KEANAKAKOI

Keanakakoi crater (Figure 2) is located approximately 1.4 km SE of Halemaumau and is 36.6 m deep. The surface dimensions of the crater are:

major axis - 459 m;
minor axis - 304 m;
mean diameter - 382 m;
aspect ratio - 0.66.

Uncertainties in surface dimensions are: $\pm$ 10 m. The floor dimensions are:

major axis - 384 m;
minor axis - 228 m;
mean diameter - 306 m;
aspect ratio - 0.59.

Uncertainties in floor dimensions are: $\pm$ 10 m. The calculated volumes for Keanakakoi are:

elliptic - $3.26*10^6$ m^3;
circular - $3.40*10^6$ m^3;
frustum - $3.41*10^6$ m^3;
mean - $3.36*10^6$ m^3.

Uncertainties in the mean volume estimates are: $\pm$ $0.2*10^6$ m^3.

Tangent to the southern edge of Keanakakoi is a major eruptive fissure oriented N78°E, which was last active in September, 1974. This fissure is considered one of this crater's present bounding faults. The northern edge of the crater appears to be coincident with a fault visible on the NW end of the crater and parallel to the Crater Rim Road. This appears to be the other present bounding fault and trends N70°E.

Figure 2. Keanakakoi crater. The aerial photograph of Keanakakoi reveals the elongated nature of the crater and the system of subparallel fractures bounding the northern and southern ends of the crater, and intersecting the central portions of the crater. Note the encroachment of the talus piles onto the surface of the September, 1974 lava lake. Scale - 1:3800. Vertical margins of the photograph are oriented N-S. (Air Survey, Hawaii, aerial photograph E-2, December, 1979. Courtesy of the Hawaiian Volcano Observatory, U. S. Geological Survey.)

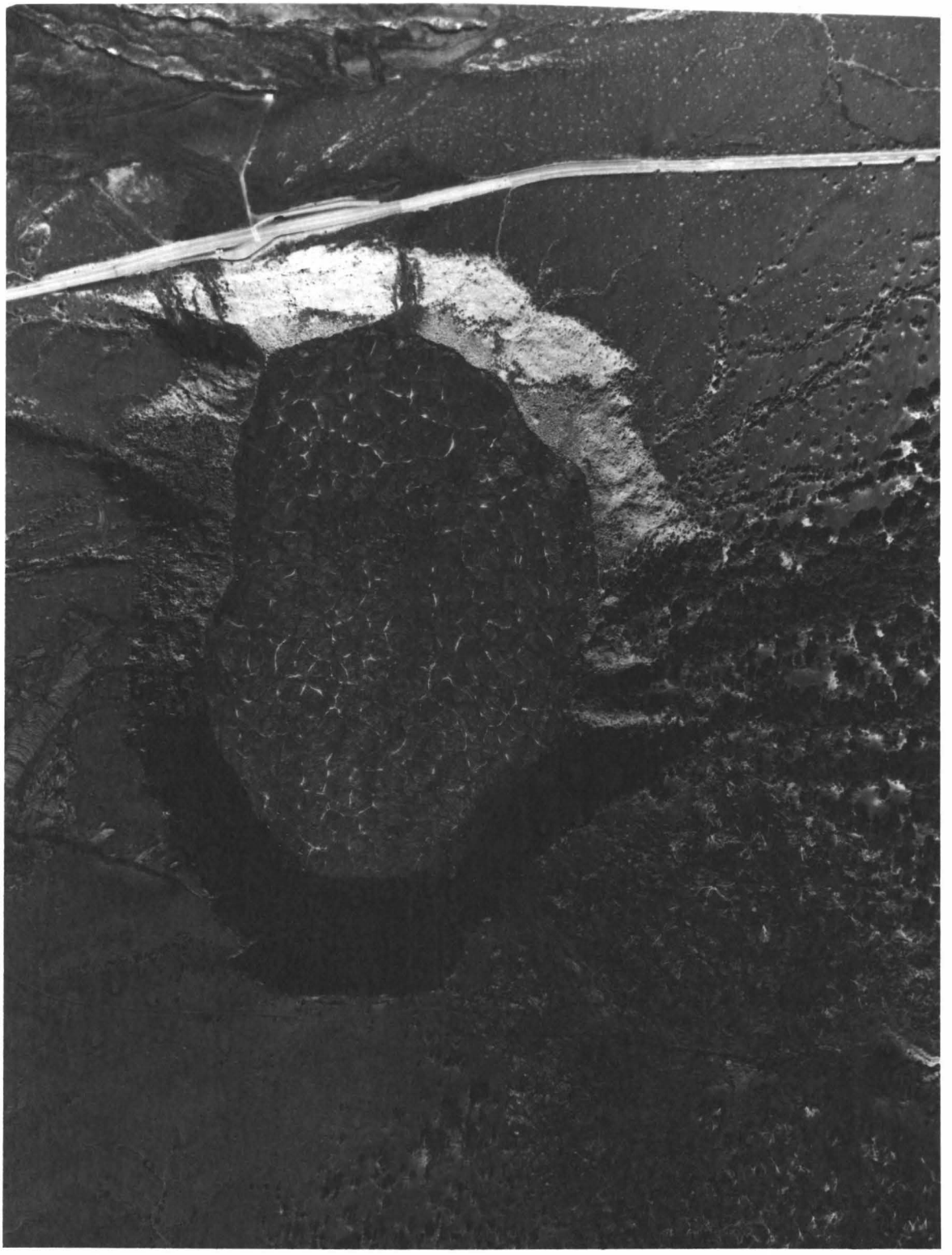

The major axis of the crater is oriented NNW.

Several fractures are located on the NE and SW sides of the crater. The fractures on the SW side are easily identifiable by the sequence of downdropped blocks defined by these fractures. Those on the NE side intersect the crater such that they act as local drainage centers and, consequently, appear as hanging gullies.

During the September 1974 eruption four eruptive vents and fissures near and in Keanakakoi contributed to a lava lake within the crater, raising the crater floor approximately 6 m above the 1877 lava lake level. A small fissure, oriented N80°E, on the SW side of the crater produced a very small lava flow which contributed a minor amount of lava drapery to the crater wall and a very small volume to the lava lake. An extension of this fissure apparently opened as a vent at the southern end of the crater floor. A small cone was built and has since collapsed, exposing a highly oxidized, ocher colored interior. This vent was probably responsible for most of the lava which formed the lake. Another eruptive fissure, approximately 50 m south of the crater and oriented N78°E, produced a large amount of lava which flowed SE into the forest, east toward Lua Manu crater and north toward Keanakakoi. The lava from this vent added a considerable amount of drapery to the crater's SE wall and may have added a significant amount of lava to the lake, judging from the extent of the drapery. On the northern side of Keanakakoi, across the Crater Rim Road, is an additional set of eruptive fissures. Although most of the lava emitted from these vents cascaded into Kilauea caldera, a small flow did cross the road and contribute

some material to the lava lake, leaving some lava drapery along the northern wall.

The lava lake, in it's cooling process, has left numerous thermal fractures on it's surface. Also, a "bathtub ring" of lava, elevated several meters above the adjacent floor is clearly visible.

Talus piles are evident around most of the crater, the larger of which are located near the intersections of the older bounding faults with the crater. Movement of older talus piles well onto the lava lake surface suggests that collapse of the crater's walls and rim has continued since the 1974 eruption.

Vegetation in Keanakakoi is limited to the NE and eastern walls. A fairly dense forest of ohia trees lies on the eastern side of the crater and is centered around the hanging gullies.

Because Keanakakoi lies very near the summit caldera it is believed that the bounding faults are related to the caldera circumferential fracture system. Orientations of the bounding faults, both old and new, are very similar to the orientation of the caldera wall just north of Keanakakoi and to the faults which define the SE portion of Kilauea caldera. Furthermore, the major axis of Keanankakoi is normal to the trend of the bounding faults; suggesting that enlargement of the crater, laterally, is determined primarily by the collapse of crater walls parallel to the faults' trends.

LUA MANU

Lua Manu crater (Figure 3) is situated 2.7 km ESE of Halemaumau. It is the first pit crater encountered to the southeast on the Chain of Craters Road and is approximately 0.7 km from the intersection of the Chain of Craters Road with the Crater Rim Road.

Lua Manu is 16.5 m deep. The surface dimensions are:

major axis - 110 m;
minor axis - 83 m;
mean diameter - 97 m;
aspect ratio - 0.75.

Uncertainties in surface dimensions are: $\pm$ 5 m. The floor dimensions are:

major axis - 83 m;
minor axis - 63 m;
mean diameter - 73 m;
aspect ratio - 0.76.

Uncertainties in floor dimensions are: $\pm$ 5m. The various calculated volumes of the crater are:

elliptic - $9.3*10^4$ m^3;
circular - $9.3*10^4$ m^3;
frustum - $9.4*10^4$ m^3;
mean - $9.3*10^4$ m^3.

Uncertainties in volumes are: $\pm$ $1.0*10^4$ m^3.

Due to the September, 1974 lava flow which covers most of the area north of the crater, Lua Manu does not present as much exposed structure, with respect to bounding faults, as does Keanakakoi. Also, any fractures that may have existed to the east of the crater have been

Figure 3. Lua Manu crater and the neighboring eruptive vents of September, 1974. The set of fissures across the Chain of Craters Road may represent an extension of the crater's northern bounding fault. At the SE end of the crater the walls are collapsing along a set of fractures that form the southern bounding fault and has left the walls nearly straight. Vertical margins of the photograph are oriented N-S. Scale - 1:2100. (Air Survey, Hawaii, aerial photograph D-1, December, 1979. Courtesy of the Hawaiian Volcano Observatory, U. S. Geological Survey.)

obscured by the contruction of the Chain of Crater Road.

Field work around Lua Manu revealed numerous circumferential fractures - fractures locally parallel to the crater's edge. On the western side of the crater however no fractures that could be interpreted as "bounding faults" were observed.

The southern end of Lua Manu's crater wall appears to be defined, in part, by a straight fracture. On both sides of this straight segment are fractures that have an orientation of N69°E. These cracks, which are probably part of one major fracture system (the southern bounding fault), have the effect of detaching large sheet-like sections of rock from the crater's walls, letting them rotate inward toward the crater's center. A second effect of these fractures is the allowance of preferential mass wastage of material along the fracture length, leaving two sections of surrounding ground rotating in toward the southern end of the crater.

Approximately 80 m east of Lua Manu is a set of fissures activated during the September, 1974 eruption. The general trend of these fissures is due east. Most of the lava from these fissures flowed south, however a small amount of lava has cascaded into Lua Manu, leaving a narrow section of drapery on the eastern wall.

The lava lake in Lua Manu is composed almost entirely of lava that flowed into the crater from the NNW side. This lava emanated from the fissures south of Keanakakoi. The cooling of the lava lake has left thermal fractures on the lake's surface. A bathbub ring approximately 8 m high on the crater's walls suggests that a considerable amount of

drainback occured.

Vegetation within the crater is sparse and limited to the region between the crater rim and the top of the prominent bathtub ring. Vegetation consists of bushes and staghorn ferns with some larger ohia trees growing out through cracks in the crater walls.

PUHIMAU

Puhimau crater (Figure 4) is located approximately 1.4 km from the Crater Rim Road - Chain of Craters Road intersection. The major axis of this crater trends N49°W, pointing directly to the center of Kilauea caldera.

The deepest point in Puhimau is approximately 159 m. The surface dimensions are:

major axis - 281 m;
minor axis - 191 m;
mean diameter - 236 m;
aspect ratio - 0.68.

Uncertainties of measurements are about ± 10 m. There is no lava lake in the crater, thus, no floor dimensions are given. The volume of Puhimau, obtained using the formula for an inverted cone, is $2.32*10^6$ m^3 ± $0.2*10^6$ m^3.

There is no field evidence of any recent eruptive activity in or around Puhimau. The area surrounding the crater is heavily vegetated. The closest fresh lava flows are from the September 1974 fissures near Lua Manu. These flows terminate about 200 m from the NW end of the crater in an asymmetric graben whose axis trends N30°E.

The area to the NE side of Puhimau contains numerous steam vents which may be connected at depth to a steaming area within Puhimau at the base of the crater's NE wall. Another steaming area, known as the Puhimau "hot area", is located approximately 400 m south of the crater.

Circumferential fractures are numerous around Puhimau, but none

Figure 4. Puhimau crater. The lava flow NNW of the crater is from the September, 1974 fissures near Lua Manu. The white regions to the NE and SW are steaming areas that presumably delineate a major fracture system oriented subparallel to the graben against which the September, 1974 flow has terminated. The crater is free of any recent lava flows; activity is limited to steaming along the NE wall. Massive talus slopes give the crater floor a funnel-like configuration, when viewed in oblique perspective. Vertical margins of the photograph are oriented N-S. Scale - 1:3100. (Air Survey, Hawaii, aerial photographs C-1 and C-3; December, 1979. Courtesy of the Hawaiian Volcano Observatory, U. S. Geological Survey.)

were observed farther than 10 m from the crater's edge. The abundance of vegetation has obscured any definite traces of bounding faults in the surrounding area. However, much like the situation at Lua Manu, a straight segment of crater wall, defined by N60°E fractures, is located at the SSE end of the crater. The lower portions of this straight segment retain and exhibit the remains of other sheet-like slabs of rock whose upper portions have rotated and collapsed into the crater.

There are no noticable talus piles along the SSW portion of the crater (beneath the tourist overlook). Large talus piles do, however, exist along the remaining crater walls. The talus piles along the NW and SE walls extend upward to within 30 m of the crater's rim. The talus piles appear to have existed for some time, as suggested by the number and size of ohia trees growing on them. There is a particular concentration of trees along the line of overlapping talus piles. Presumably, these piles are still actively growing, although the growth rate is believed to diminish as the piles approach the crater rim.

Vegetation within Puhimau is fairly abundant; particularly in the area above the steam vents, including staghorn ferns and oheluberry bushes, scattered throughout the crater.

KOKOOLAU

Kokoolau crater is located approximately 0.8 km SE of Puhimau. The crater is not easily visible from the Chain of Craters Road due to dense vegetation.

The crater is small, approximately 130 m in diameter and slightly elongated toward the northwest. A depth of 18 m and a floor with a diameter of 50 m have been estimated through analysis of aerial photographs and topographic maps. A volume of approximately $0.11*10^6$ m^3 has been derived by averaging the volumes calculated using the circular, elliptic and frustum formulae. This fits well as a member of the group of small pit craters consisting of Lua Manu and Devil's Throat. Kokoolau has a hummock extending from the western wall in towards the center, decreasing in height. This hummock may be a neck of ground separating what could be two distinct collapse areas. On the western side of the crater, south of the hummock, is a fault scarp trending SW-NE with the north side dropped down. Airphoto examination suggests that the fault scarp extends a considerable distance westward toward the Koae fault system. No evidence of this fault scarp exists on the eastern side of Kokoolau.

The entire area within and around Kokoolau is covered by a dense canopy of mature ohia trees. The amount of vegetation on the talus slopes indicates that these slopes have reached an angle of repose and that the interior walls of the crater have stablized, despite the existence of several sections of vertical crater wall exposed in the southern end.

HIIAKA

Hiiaka crater (Figure 5) is part of a large complex of fault scarps and fault blocks located about 1.4 km SE of Kokoolau crater. Examination of airphotos and topographic maps indicates that these faults and scarps are a part of the Koae fault system. Hiiaka crater, then, is situated at the intersection of the Koae fault system with the upper east rift zone.

Hiiaka crater is 94.5 m deep and is nearly circular (surface aspect ratio: 0.98). The surface diameter is 373 m (± 10 m) and the floor diameter is 119 m (± 10 m). The different calculated volumes are:

elliptic - $5.69*10^6$ m^3;
circular - $4.49*10^6$ m^3;
frustum - $4.89*10^6$ m^3;
mean - $5.02*10^6$ m^3 (± $0.2*10^6$ m^3).

Hiiaka crater is situated at the east end of a larger subsidence complex forming a crater within a large depression. A system of normal faults with north facing scarps have been identified from field observations and aerial photography. The scarps have been designated, starting from the crater's southern edge, as scarp A through scarp D. Scarp A (Figure 5) begins at the south end of Hiiaka crater and initially trends WSW toward the Chain of Craters Road. This fault then changes direction toward the NW, defining a gently curving scarp, approximately 8 m high, extending around Hiiaka crater until it coalesces with a gently sloping region to the NW. The area between this scarp and Hiiaka forms a plateau and varies in width from several meters

Figure 5. Hiiaka crater lies at the eastern end of a complex of normal faults with north-facing scarps. These faults and scarps, part of the Koae fault system, define a large, asymmetric depression and form the crater's present southern bounding fault. Evident in the airphoto are the fissures of the May 5, 1973 eruption, their lava flows and the lava lake that has formed in Hiiaka. Note the large "bathtub ring" above the lake surface, suggesting large scale drainback. Note, also, the massive amounts of talus on all sides of the crater. Vertical margins of the photograph are oriented N-S. Scale - 1:4800. (Air Survey, Hawaii, aerial photograph F-1a; December, 1979. Courtesy of the Hawaiian Volcano Observatory, U. S. Geological Survey.)

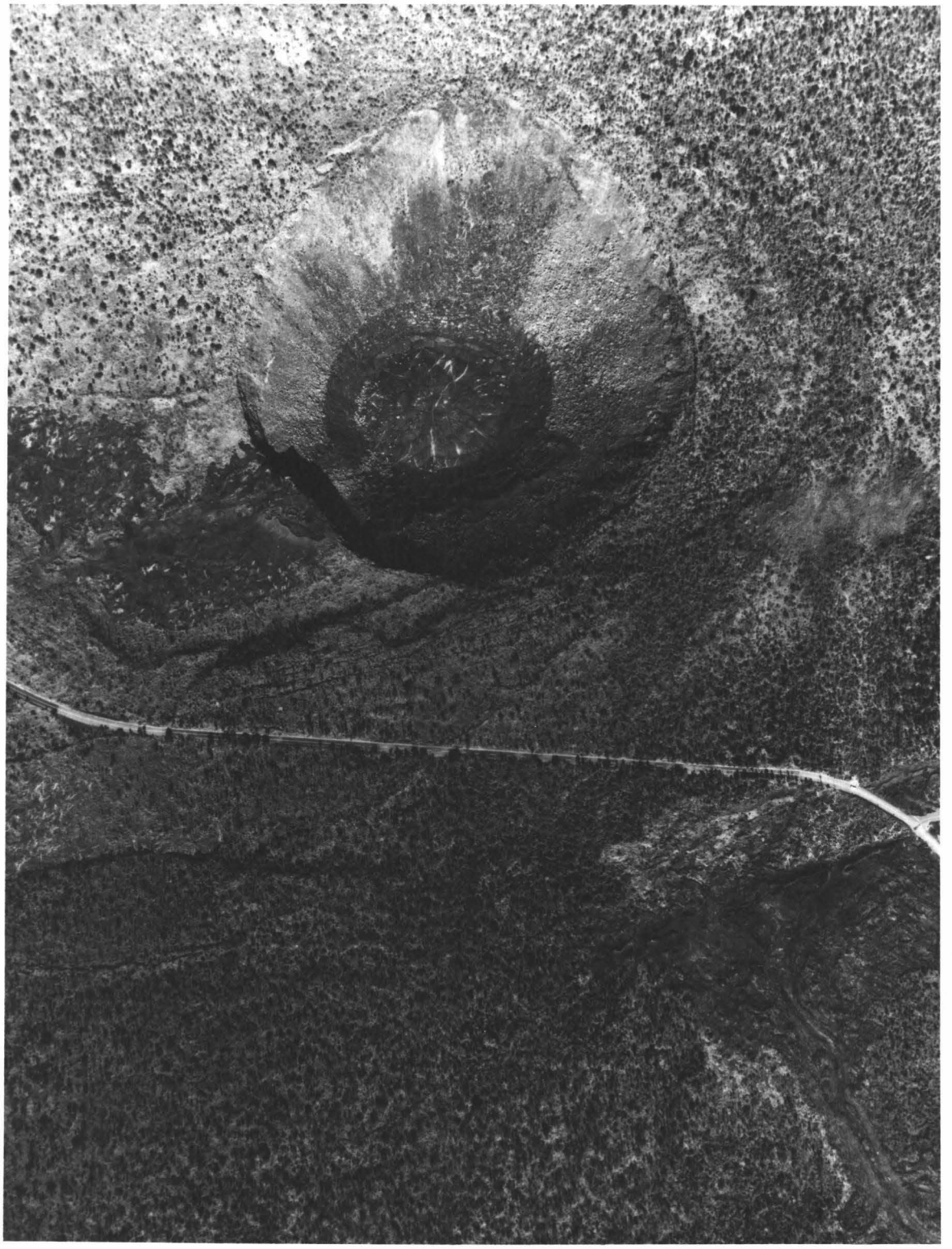

near the SW end to nearly 120 m NW of the crater's rim.

The southern end of Hiiaka formed by scarp A, bounds another scarp (B) that rises about 17 m above A. Behind scarp B is yet another scarp (C) that rises about 6 m above scarp B. Scarp C is the result of displacement along a fault that is visible for several tens of meters west of the Chain of Craters Road, extending eastward toward the southern end of Hiiaka. This fault appears to continue around the eastern and northern sides of the crater where it is defined by a semi-circular ridge which rises above the crater. This ridge terminates NW of Hiaaka, where it dissipates into an area of higher elevation. The region bounded by scarp C and scarp D contains numerous small fractures oriented N70^{o}E. Scarp D is clearly visible west of the Chain of Craters Road and trends N80^{o}E. This scarp disappears gradually as it heads toward Pauahi crater.

In May, 1973 a series of eruptive fissures and vents opened in and near Hiiaka and Pauahi craters. The amount of erupted lava was sufficient to destroy large areas of ohia forest, in addition to forming lava lakes in both Hiiaka and Pauahi.

An eruptive fissure about 120 m long, oriented east-west, and located approximately 800 m west of Hiiaka produced a lava flow that travelled south, ponding and terminating against scarp D. This fissure also produced a flow that crossed the Chain of Craters Road, cascaded over scarp A, covered portions of the plateau and may have cascaded into Hiiaka crater.

A second fissure opened on the plateau with a primary vent near

scarp A. This fissure trended N65°E and may have intersected the western wall of Hiiaka. Lava from this fissure cascaded over the crater's edge, contributing to the lava lake.

A short SE-oriented fissure opened very near the SW rim of Hiiaka. The non-eruptive extension of this fissure clearly fractures the southern wall of the crater. This fissure acted as both an eruptive source and a drainback crack. The orientation of this fissure suggests that it is not a bounding fault or typical N60°E - N70°E fracture, but is a circumferential fracture that provided an additional means of transporting magma to the surface. An additional fissure, oriented N70°E, opened on the southern talus slope of Hiiaka. This fissure produced most of the lava that filled in the crater floor.

The upper third of the crater has walls that are nearly vertical. The remainder of the crater is a massive funnel-shaped assemblage of coalesced talus piles. Large blocks of the former crater wall, up to 6 m across, are visible on the lava lake surface.

A bathtub ring that formed during the August, 1968 eruption (Jackson and others, 1975) is still visible and rises approximately 20 m above the current lake level.

The vegetation around Hiiaka ranges from the desert type of flora in the west to dense ohia forests to the south and east. Virtually no vegetation is visible within the crater except for scattered patches of grasses and ferns.

PAUAHI COMPLEX

The Pauahi area is large and contains three distinct regions of collapse; Pauahi North, Pauahi South and Pauahi East (Figure 6). The bounding faults and fractures in these regions are less obvious than those in the Hiiaka area. Lava lakes were formed in Pauahi North and Pauahi South during the May 5, 1973 eruption; and a small flow began to fill Pauahi East. The lavas of the November 16-17, 1979 eruption effectively covered the lava lakes of Pauahi North and Pauahi South.

The lateral measurements for Pauahi North and Pauahi South are approximations, since the two craters overlap. These approximations were obtained by continuing the curvature visible in one crater into the void space of the other crater and measuring the projected axial lengths.

1. Pauahi North

Pauahi North is situated 400 m SE of Hiiaka crater. The southern and SE walls are missing; this being the area that coalesces with Pauahi South.

The depth of Pauahi North, from the crater edge to the surface of the November 1979 lava lake, is about 108 m. The surface dimensions are:

major axis - 270 m;
minor axis - 265 m;
mean diameter - 267 m;
aspect ratio - 0.98.

Figure 6. The Pauahi complex. The complex consists of northern and southern pits (Pauahi North and Pauahi South) and a circular crater of shallower depth to the east of the southern pit (Pauahi East). The dense vegetation surrounding the complex has obscured older, structural and eruptive features. The May, 1973 eruptive fissures are evident along the northern edge of the complex and north of Pauahi East. A small fissure of the same period is seen on the NE slope of Pauahi South. The November 16, 1979 fissures are on the NW wall of Pauahi North and extend across the Chain of Craters Road, parallel to and south of the May, 1973 fissures. The lava ponds are capped by lava of November, 1979. Note the minimal amount of talus in Pauahi North, the relatively large amount of talus in Pauahi South and the overgrown nature of Pauahi East. The vertical margins of the photograph are oriented N85°E. Scale - 1:3500. (Air Survey, Hawaii, aerial photographs 3-7 and 3-8; December 1979. Courtesy of the Hawaiian Volcano Observatory, U. S. Geological Survey.)

Uncertainties in these dimensions are: ± 10 m. The floor dimensions are:

major axis - 174 m;
minor axis - 130 m;
mean diameter - 152 m;
aspect ratio - 0.75.

Uncertainties in these dimensions are: ± 10 m. The calculated volumes of the crater are:

elliptic - $3.99*10^6$ m^3;
circular - $3.72*10^6$ m^3;
frustum - $3.81*10^6$ m^3;
mean - $3.84*10^6$ m^3.

Uncertainties in the volume estimates are: ± $0.2*10^6$ m^3.

Along the northern edge of the crater is a fissure (N74°E) from the May 1973 eruption. This fissure extends WSW across the Chain of Craters Road. Approximately 20 m south of this extension is a parallel fissure from the November, 1979 eruption.

At the northern end of Pauahi North are three vents, mid way up the crater wall, that align themselves N70°E. The central vent is the primary eruptive vent of November, 1979.

Several major cracks can be seen in the eastern wall of Pauahi North. Judging from the orientation of blocks separated by these cracks, the cracks appear to be oriented N70°E. Several large cracks are also visible in the western wall trending SW.

The floor of Pauahi North is separated from Pauahi South by a narrow rampart over which the 1979 lavas flowed. The western side of this rampart joins a fragment of Pauahi North's southern wall. This

portion of the wall is linear, suggesting a bounding fault origin, and is oriented N73°E. An extension of a bounding fault in this area would coincide exactly with a set of 1973 fissures east of Pauahi South and north of Pauahi east.

A peculiar feature common in Pauahi North is the terrace wall construction on the eastern and western sides. These walls exhibit alternating areas of vertically cut walls and high angle talus slopes. The vertical sections are generally composed of thick flow units, while the talus slopes obscure the stratigraphy.

Vegetation in Pauahi North is limited to patches of various grasses growing on the short talus slopes on the eastern wall. The entire region surrounding the Pauahi complex is heavily forested; except in the areas overrun by the eruptions of 1973 and 1979.

2. Pauahi South

Pauahi South appears to be greatly elongated in the NW-SE direction. This is because the lava lake is oval in plan view. Measurements of various surface diameters reveal that Pauahi South is, in fact, nearly circular.

The depth of Pauahi South, from the crater edge to the November 1979 lava lake surface, is 113 m. The surface dimensions are:

major axis - 384 m;
minor axis - 372 m;
mean diameter - 378 m;
aspect ratio - 0.97.

Uncertainties in these dimensions are: ± 10 m. The floor dimensions

are:

major axis - 198 m;
minor axis - 105 m;
mean diameter - 152 m;
aspect ratio - 0.53.

The uncertainties are: ± 10 m. The calculated volumes of the crater are:

elliptic - $6.24*10^6$ m^3;
circular - $6.23*10^6$ m^3;
frustum - $6.61*10^6$ m^3;
mean - $6.36*10^6$ m^3.

And the uncertainties in these volume estimates are: $\pm$ $0.2*10^6$ m^3.

Although no definitive bounding faults were discovered on the south end of Pauahi South, topographic maps show several major faults to the SW oriented N70°E. Extension of these cracks would be tangent to the SE end of Pauahi South.

A portion of Pauahi South's east rim is a ridge that separates Pauahi South and Pauahi East. This ridge is also lower in elevation than the surrounding rim.

On the NE wall of Pauahi South, and extending eastward on the surface, is a set of May 1973 eruptive fissures. Lava appears to have flowed from these fissures onto the crater floor. The western end of the fissures halts abruptly at an exposed, thick flow unit. Lava flowing down the talus pile may have carried some of the loose talus with it; leaving the underlying, older crater wall exposed.

The lava lake that formed as a result of the 1973 eruption left a bathtub ring that is exposed on all sides of the crater, except in the

west, where recent talus piles have covered it. The bathtub ring is approximately 15 m high and suggests large-scale drainback.

Large talus piles appear on all sides of the crater. In fact, the talus piles on the southern end of Pauahi South are mature enough to have reached an angle of repose and to have allowed fairly dense growths of ohia trees to take place. In constrast, the eastern, western and northern talus piles have little vegetation.

3. Pauahi East

Pauahi East is a small crater sharing a common ridge with Pauahi South. Like Kokoolau, this crater is overgrown with large numbers of trees and assorted vegetation. No fresh talus piles are seen anywhere in the crater.

The north side of Pauahi East is partially covered by the lava of May 1973. The N70^{o}E fissures lie only 30 m to the north. Analyses of topographic maps and airphotos suggest that this crater has approximate dimensions as follows:

depth = 40 m;
radius = 100 m;
aspect ratio = 1.0;
volume = $0.4*10^{6}$ m^{3}.

Uncertainties in these measurements are: + 5 m, $\pm$ $1.0*10^{4}$ m^{3}.

Like the elongated craters near the summit (Keanakakoi, Lua Manu and Puhimau), the combined axes of Pauahi North and Pauahi South point toward Kilauea's summit. The combined axes of Pauahi South and Pauahi East, interestingly, are oriented approximately N70^{o}E.

III. DEVIL'S THROAT

Devil's Throat (Figure 7) is a very small pit crater on Kilauea's upper east rift zone approximately 150 m east of the Chain of Craters Road and Hilina Pali Road intersection. The area surrounding Devil's Throat is sparsely vegetated and shows no signs of recent eruptive activity.

Devil's Throat is thought to be the newest pit crater on the upper east rift zone, believed to have formed in 1921 (Macdonald and Abbott, 1977); however, no evidence in other literature of the period indicates a definite date of formation. Jaggar (1947) mentions Devil's Throat as a pit crater that opens wider downward, and deformation maps of the period suggest that Devil's Throat was in existence at least by 1921 (Wilson, 1935). By the mid 1960's, Devil's Throat may have had a much smaller diameter than that at present, with overhanging crater walls (A. Okamura, personal communication) providing a small diameter.

Regardless of the precise year when Devil's Throat first broke through to the surface, it appears to be much younger than the other craters in the upper east rift zone.

FIELD MEASUREMENTS

A plumb line was lowered to the bottom of Devil's Throat and the amount of line paid out was measured, giving a depth of 50.6 m. The same line was extended across Devil's Throat several times giving an average diameter of 43.4 m. The amount of error in these measurements

Figure 7. Devil's Throat. This crater of right circular geometry, is the youngest pit crater in the study area. The lack of eruptive activity has preserved the ground cracking believed to be associated with the crater's formation. The southern bounding fault is well defined to the SW but diffuse to the NE. The northern bounding fault is only vaguely defined to the SW but more apparent to the NE (see also Fig. 8). About 130 m NW of the crater is a system of left-stepping en echelon fractures. This system and the southern bounding fault are believed to be part of the Koae fault system. The vertical margins of the photograph are oriented N-S. Scale - 1:2900. (Air Survey, Hawaii, aerial photograph F-2; December, 1979. Courtesy of the Hawaiian Volcano Observatory, U. S. Geological Survey.)

is believed to be no greater than 1 m.

The walls of the crater are vertical, giving an apparent break angle of 90^{o}. Thus, the crater is nearly a right circular cylinder with a volume of 7.48×10^{4} m^{3}.

The distribution and orientations of the fractures around Devil's Throat were also determined. Eleven unevenly spaced rays were extended outward from the crater's edge. Along these rays, the radial distances of the intersected circumferential fractures were measured as well as the crack opening displacements. Figure 8 shows the locations of the rays and Table I contains the results.

In addition, two baselines, on the north and south sides of the crater, were established from which perpendicular lines at evenly-spaced intervals from a common datum were laid down and the locations and amounts of the crack opening displacement of other major fractures recorded. Figure 8 and Table II show the configuration of the arrays and the measurements, respectively. The two baselines were superimposed over the apparent bounding faults. Not unexpectedly, the orientation of nearly all the fractures beyond the circumferential fractures was between $N60^{o}E$ and $N80^{o}E$.

Throughout the crack distribution study care was taken so that individual fractures near the crater were not counted in both the radial array and the grid array.

Two additional studies of Devil's Throat were conducted utilizing a photograph of the crater in which a stadia rod for scale is visible (Figure 9). The average flow thickness was determined by using a pair

Figure 8. A sketch map of Devil's Throat showing the distribution of cracks around and near the crater. The lightly shaded areas are zones of intense ground cracking. The darker shaded zones adjacent to the crater are sagging, unstable areas that are partially detached from the surrounding rock. The numbers within the crater refer to the rays and measured circumferential cracks in Table I. The two sets of four traverses each refer to the data in Table II. The trees on the north and south sides of the crater are references points for the North Base Line and South Base Line, respectively. Note the subparallel nature of the cracks around the crater and the fracture system to the NW.

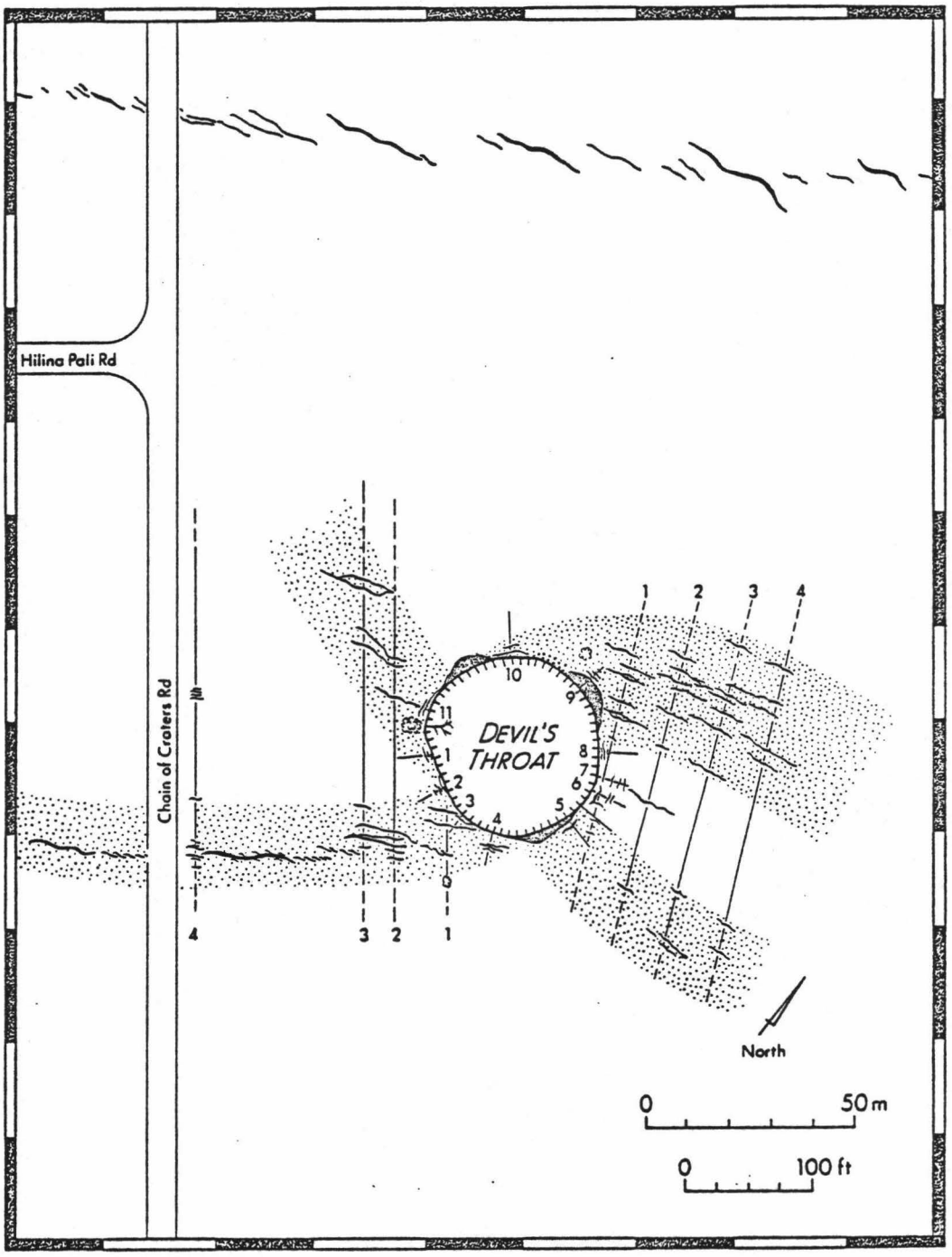
Hilina Pali Rd
Chain of Craters Rd
DEVIL'S THROAT
1
2
3
4
North
0
50 m
0
100 ft

Table I. Devil's Throat Crack Analysis (I). The radial distribution and dilation of the circumferential fracture system.

Ray #1		Ray #2		Ray #3		Ray #4	
r (m)*	cod (cm)+	r (m)	cod (cm)	r (m)	cod (cm)	r (m)	cod (cm)
0.2	2.5	0.9	3.5	1.1	19.	3.0	8.5
0.7	3.0	1.1	5.0			3.6	22.0
1.0	1.0	1.3	2.0			4.4	16.0
1.7	8.5	1.8	1.5				
		2.8	1.0				

Ray #5		Ray #6		Ray #7		Ray #8	
r (m)	cod (cm)	r (m)	cod (cm)	r (m)	cod (cm)	r (m)	cod (cm)
1.3	7.	1.6	26.	4.0	7.	0.8	14.
2.1	16.	4.3	4.5	5.7	2.	1.5	22.
		5.2	5.	6.6	3.	2.0	4.

Ray #9		Ray #10		Ray #11	
r (m)	cod (cm)	r (m)	cod (cm)	r (m)	cod (cm)
0.5	33.	0.8	18.	0.9	2.
3.3	6.	2.2	3.5	1.4	5.
4.3	7.				
5.2	3.5				
6.7	3.				

* r: distance from crater edge
\+ cod: crack opening displacement

Table II. Devil's Throat Crack Analysis (II).
The distribution and dilation of the neighboring en echelon fracture system.

North Base Line: N65°E from tree

Traverse #1		Traverse #2		Traverse #3		Traverse #4	
d (m)*	cod (cm)+	d (m)	cod (cm)	d (m)	cod (cm)	d (m)	cod (cm)
-2.0	4.0	-4.2	6.0	-9.5	4.0	-6.4	10.
0.9	5.0	-0.8	4.0	0.0	5.0	1.5	4.5
2.9	6.5	1.7	7.0	2.4	6.0	4.4	3.0
4.1	6.0	3.8	5.0	3.8	5.0	11.6	5.0
9.8	6.5	9.8	4.5	9.1	3.5	16.3	8.0
12.5	7.0	17.7	6.0	11.3	11.0	56.1	3.5
13.8	7.0	31.7	14.	21.0	4.0	62.5	4.5
18.6	4.0	53.3	9.0	51.2	3.0		
34.4	6.0			62.8	6.0		
38.7	6.0			66.5	5.5		
46.9	14.						

South Base Line: N52°E from tree

Traverse #1		Traverse #2		Traverse #3		Traverse #4	
d (m)	cod (cm)	d (m)	cod (cm)	d (m)	cod (cm)	d (m)	cod (cm)
5.5	7.0	4.9	13.0	5.9	6.0	3.5	10.0
13.1	7.0	6.9	30.0	8.0	36.0	5.2	6.0
16.8	18.0	8.5	10.5	8.7	7.0	6.1	32.0
		9.8	7.0	11.3	10.0	8.1	22.0
		12.0	5.0	14.0	6.0	8.6	11.0
		43.9	14.0	54.6	29.0	9.3	10.0
		51.2	29.0	58.2	6.0	20.4	6.0
		53.3	7.5	68.0	14.0	44.2	10.0
				70.4	8.0	45.1	4.0
						45.7	9.0
						46.3	2.0

* d: distance from base line
\+ cod: crack opening displacement

Figure 9. Devil's Throat Section. The photograph shows the NW wall of Devil's Throat used to determine the average flow unit thickness and the average joint spacing. The stadia rod is twelve feet high and each one foot interval is subdivided into tenths of a foot.

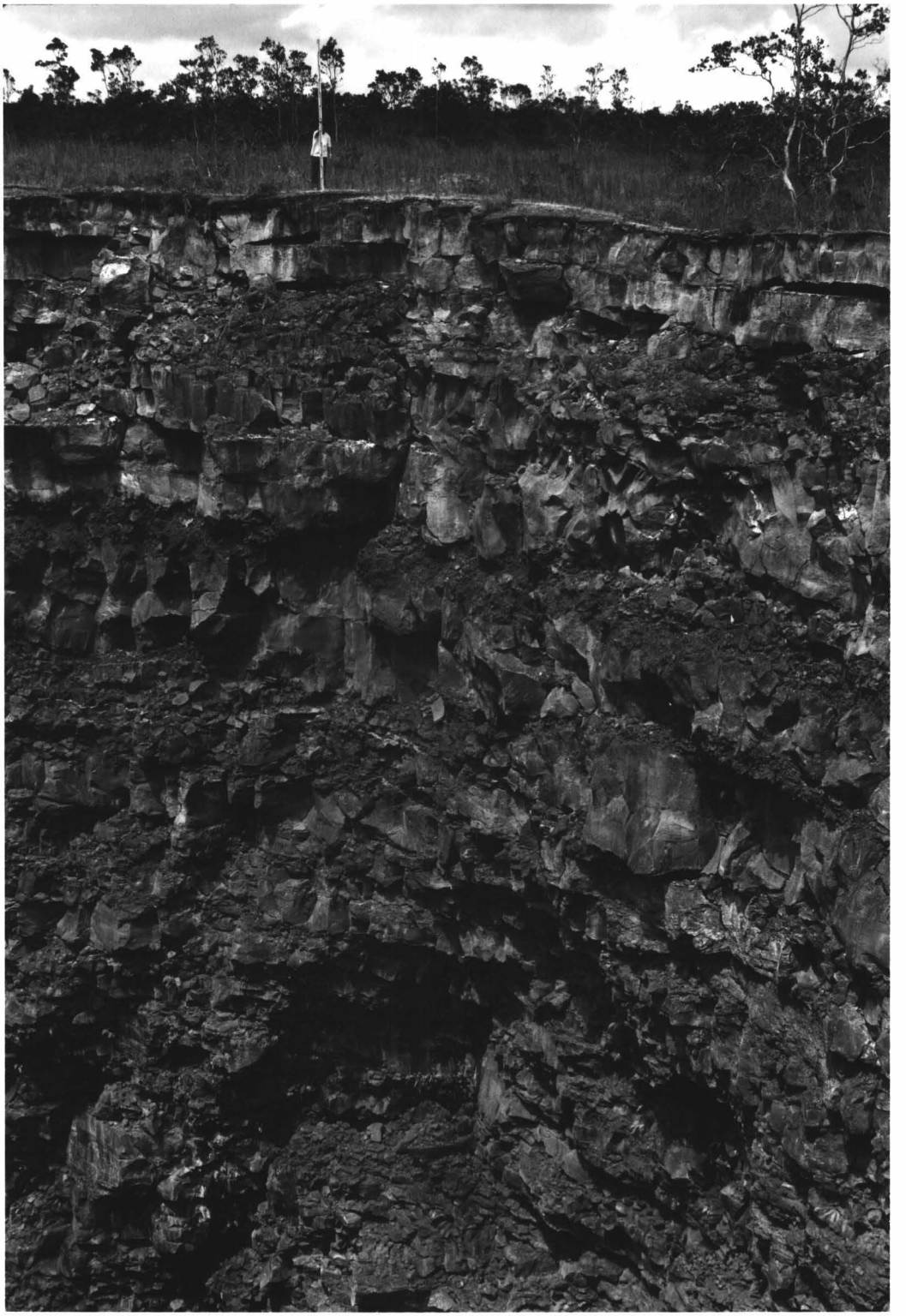

of needle point dividers to establish the scale of the photographs and to measure individual flow thicknesses (exclusive of aa layers). The top five flow units were measured, and the results are provided in Table III.

Subvertical joint spacings were obtained by the same method using only the top six flow units. No measurements were taken more than ten meters from the vertical line defined by the stadia rod due to foreshortening distortion produced by the curvature of the crater wall. The joint spacings are given in Table IV.

The bounding fault on the south side of Devil's Throat has been traced westward across the Chain of Craters Road, through dense vegetation and across the Hilina Pali Road, at which point it is apparent that the fault merges with the Koae fault system. A small scale (1:2900) airphoto (Figure 7) indicates that the northern bounding fault behaves similarly. Also evident in the airphoto is another N70°E fracture approximately 130 m NW of Devil's Throat.

Additional observations of Devil's Throat include:

(i) talus distributed evenly, in general, on the crater floor;
(ii) extension of the roots of a tree on the NW side of the crater some 7 m toward the crater's center;
(iii) the existence of three sagging areas on the NE, SE and western portions of the crater's rim.

DISCUSSION

The geometric and volumetric dimensions of Devil's Throat suggest that the pit crater is young. Near-vertical walls and the lack of

Table III. Devil's Throat Section - flow unit thicknesses

flow unit number	flow thickness (cm) number 1	2	3	4	5	6	7	8	9	10	average
1	93	86	93	100	93	93	106	93	93	93	94
2	106	100	106	86	100	100	93	86	93	100	97
3	120	126	113	140	113	113	113				120
4	173	200	206	200	173	219	200	180	219	206	200
5	86	100	133	140	146	126	140	100	133	133	126
										mean flow unit thickness:	127

Table IV. Devil's Throat Section - intraflow joint spacing.

flow unit number	joint spacing (cm) number 1	2	3	4	5	6	7	8	9	10	average
1	104	151	76	61	80	52	47	47	47	47	71.1
2	142	118	113	170	142	118	156			109	133.5
3	85	137	104	99	90	142	142	118	99	109	112.5
4	236	208	184	184	189	298					216.5
6	85	109	76	95	95	95	104	118	113	113	100.3
									mean joint spacing:		126.8

mature talus slopes also support this supposition.

The preservation of the fragile aa structure of the flow units exposed in the walls of the crater suggests that the crater is the result of a single collapse event.

The near-field fractures surrounding Devil's Throat are concentric to the crater. They reflect the development of tensile stresses and the resulting deformation made possible by the close presence of an unrestrained boundary (the crater wall).

The southern bounding fault appears to have had more influence in the development of the pit crater than the northern bounding fault; it is larger, more distinct and generally has larger crack opening displacements. The northern bounding fault appears to be a minor fracture that has dilated due to the lateral restraints removed by the presence of the crater.

Throughout the period from 1912 through 1921, during the development of the surface expression of Devil's Throat much attention of the staff of the Hawaiian Volcano Observatory was focused on Kilauea's summit with it's active lava lake and on the SW rift where major eruptive phases had taken place. It seems possible, then, that the initial collapse of Devil's Throat went unnoticed and seismically undetected. A possible evolutionary sequence may have taken the following form. Devil's Throat may have been in existence for many years prior to 1921 with a thin roof of only two or three flow units. The major deformation events just prior to 1921 (Wilson, 1935) may have been enough to produce a sufficient amount of tension across the roof of

the subjacent cavity, allowing the central blocks of the roof to collapse. The configuration of Devil's Throat, then, would coincide with those reported by Jaggar (1947) and Wilson (1935): a downward opening pit crater. During the next forty years, the rim of Devil's Throat presumably slowly collapsed, enlarging it's diameter but still retaining the downward-opening nature as observed by A. Okamura during the mid 1960's. Finally, in 1980, Devil's Throat is visible as a vertical, circular pit crater. The collapse of the previously overhanging portions of the crater's rim may have been due to the deformation accompanying the eruptive episodes of Mauna Ulu, a time of numerous inflation-deflation events in the area.

IV. SUBSIDENCE MECHANICS

This section outlines the elements of the subsidence mechanics model. It is based on the presentation of Berry (1960, 1963, 1964) and Berry and Sales (1961, 1962), who have derived relations for the two and three dimensional displacement fields above a cavity of prescribed dimensions.

Following Berry and Sales (1962) we consider a three-dimensional cavity of rectilinear geometry, characterized by a depth of burial h, a floor-to-ceiling height t, a width 2a and a length 2b. The cavity is embedded within a transversely isotropic half-space, employing cartesian coordinates. Figure 10 illustrates the void with the critical geometric parameters.

In general, three possible modes of cavity closure in two dimensions are considered:

(i) complete closure, where the roof contacts the floor along the entire length 2a;
(ii) partial closure, where the roof-floor contact does not extend along the entire length;
(iii) non-closure, where there is no roof-floor contact at any point along 2a.

If the depth, h, is much larger than the thickness, t; and, if complete closure is assumed, then the roof-floor contact can be treated as a "constant displacement discontinuity" or "dislocation" (Berry and Sales, 1962).

The displacement problem was initially solved for a two-dimensional, isotropic case (Berry, 1960) and, later, for a two

Figure 10. A schematic repesentation of a three-dimensional rectilinear void of width 2a, length 2b and thickness t, buried at a depth, h. The subsidence model yields the amount of vertical deformation at each nodal point of the surface Cartesian coordinate system, given the complete closure of the cavity. The x, y and z directions are model directions that correspond to the width, length and thickness directions of the cavity, respectively.

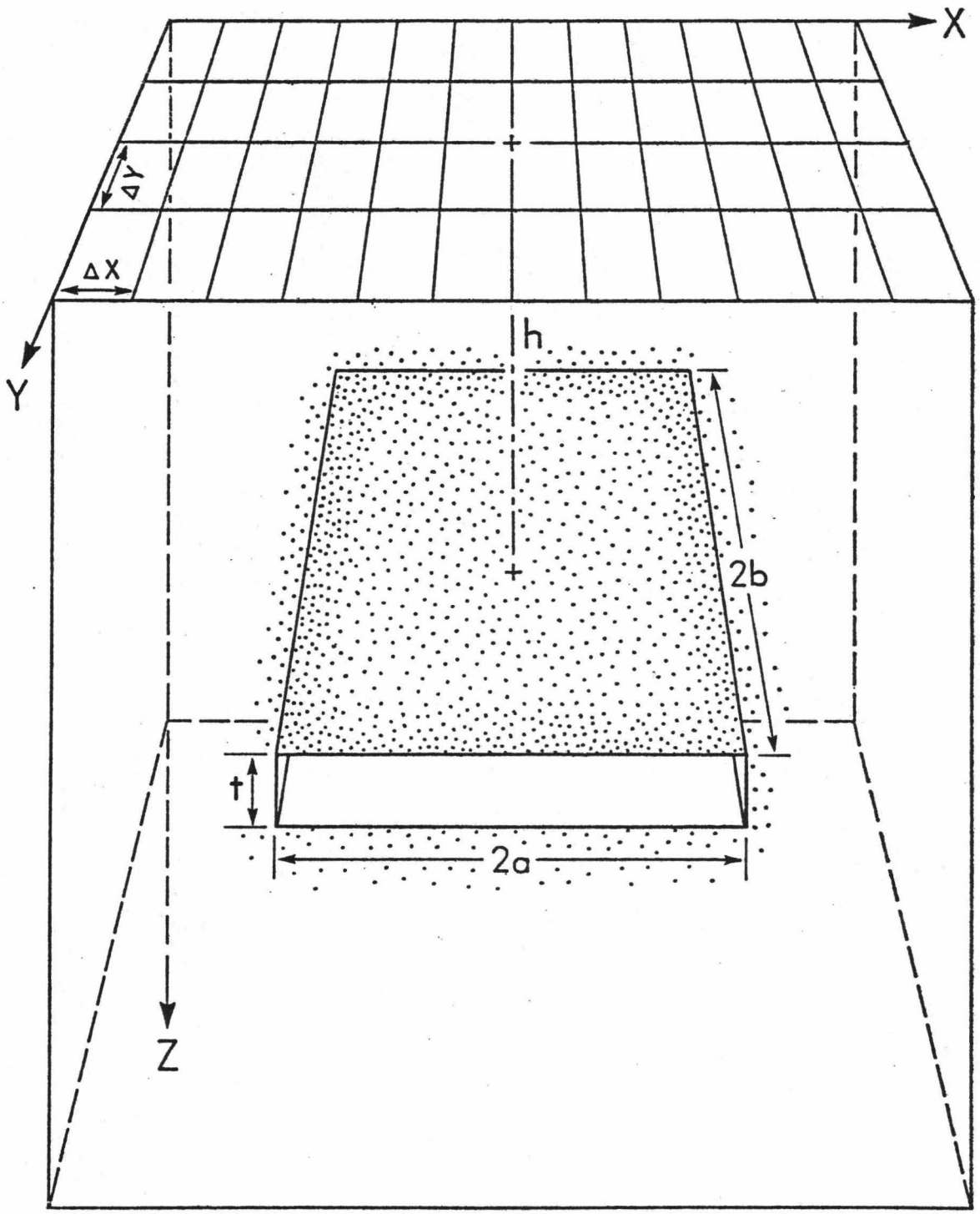
X
ΔY
ΔX
Y
h
2b
t
2a
Z

dimensional, transversely isotropic medium (Berry and Sales, 1961) and, finally, a three dimensional, transversely isotropic medium (Berry and Sales, 1962).

The solution of a three-dimensional deformation field for a transversely isotropic medium is used in this study because it allows more input of geologic data. Although only the case of complete closure has been solved analytically, the differences between the solution of the three closure cases in two dimensions are small (Berry, 1964) and within the limits of the uncertainty in the applicability of the other parameters.

The problem of solving for surface displacements in this situation can be simplified by setting the stresses and displacements to zero at infinity. The plane on which the displacement discontinuity lies is then symmetric with respect to stresses and displacements, and the z-y plane is free to act as a plane of symmetry. The medium, then, has stress-strain relationships as follows:

$$\sigma_x = c_{11}\varepsilon_x + c_{12}\varepsilon_y + c_{13}\varepsilon_z \,, \tag{5a}$$

$$\sigma_y = c_{12}\varepsilon_x + c_{11}\varepsilon_y + c_{13}\varepsilon_z \,, \tag{5b}$$

$$\sigma_z = c_{13}\varepsilon_x + c_{13}\varepsilon_y + c_{33}\varepsilon_z \,, \tag{5c}$$

$$\tau_{yz} = 2c_{44}\gamma_{yz} \,, \tag{5d}$$

$$\tau_{xz} = 2c_{44}\gamma_{xz} \,, \tag{5e}$$

$$\tau_{xy} = (c_{11} - c_{12})\gamma_{xy} \,, \tag{5f}$$

where σ_i is the stress acting in the i^{th} direction, ε_i is the strain

acting in the i^{th} direction, τ_{ij} is the shear stress acting in the ij^{th} direction, γ_{ij} is the shear strain acting in the ij^{th} direction and c_{ij} is the ij^{th} element of the stiffness matrix.

A displacement field in three dimensions can be solved if:

(i) the equations of equilibrium are satisfied;
(ii) (5) is satisfied;
(iii) no shear stresses exist on any vertical planes (i.e., $\tau_{xz} = \tau_{yz} = 0$).

The displacement field is then described by:

$$u = \frac{\partial}{\partial x} (\phi_1 + \phi_2) , \tag{6a}$$

$$v = \frac{\partial}{\partial y} (\phi_1 + \phi_2) , \tag{6b}$$

$$w = \frac{\partial}{\partial z} (q_1\phi_1 + q_2\phi_2) , \tag{6c}$$

if $\phi_1(x,y,z)$ and $\phi_2(x,y,z)$ can be expressed in terms of a single harmonic function $\Phi(x,y,z)$. Here,

$$\phi_1 = \frac{\alpha_1}{1+q_1} \Phi(x,y,z_1) , \tag{7a}$$

$$\phi_2 = -\frac{\alpha_2}{1+q_2} \Phi(x,y,z_2) , \tag{7b}$$

$$\nabla^2\Phi(x,y,z) = 0 , \tag{7c}$$

$$z_j = z/\alpha_j , \quad j=1,2. \tag{7d}$$

And, α_1 and α_2 are the positive real roots of:

$$c_{11}c_{44}\alpha^4 + (c_{13}(2c_{44}+c_{13})-c_{11}c_{33})\alpha^2+c_{33}c_{44} = 0 . \qquad (8)$$

Furthermore,

$$q_j = (c_{11}\alpha_j^2 - c_{44})/(c_{13} + c_{44}), \qquad j=1,2. \qquad (9)$$

Thus, ω and σ_z can be written as:

$$w=(\frac{q_1}{1+q_1})\frac{\partial}{\partial z_1}\Phi(x,y,z_1) - (\frac{q_2}{1+q_2})\frac{\partial}{\partial z_2}\Phi(x,y,z_2), \qquad (10)$$

$$\sigma_z=c_{44}(\alpha_1\frac{\partial^2}{\partial z_1^2}\Phi(x,y,z_1) - \alpha_2\frac{\partial^2}{\partial z_2^2}\Phi(x,y,z_2) . \qquad (11)$$

Because of the zero stress, zero displacement conditions imposed at infinity, the plane, z=0, becomes a plane of symmetry facilitating treatment of the problem using half-spaces. Thus, if t is small compared to a and b, a new set of boundary conditions arise. Using (10),

$$(\frac{q_1}{1+q_1} - \frac{q_2}{1+q_2})(\frac{\partial}{\partial z}\Phi(x,y,z))_{z=0} = \begin{cases} -1/2\ t, & |x|\leq a \text{ and } |y|\leq b \\ 0\ , & \text{elsewhere.} \end{cases} \qquad (12)$$

Then, the problem of finding an appropriate $\Phi(x,y,z)$ becomes a Dirichlet boundary value problem. The mathematical details for the

solution of $\Phi(x,y,z)$ are given by Berry and Sales (1962), and follow the treatment of Green and Zerna (1954). Berry's value of $\Phi(x,y,z)$ is:

$$\Phi = \frac{t}{4\pi} \frac{(1+q_1)(1+q_2)}{q_1-q_2} I \ , \tag{13}$$

where:

$$\frac{\partial I}{\partial x} = - \log \frac{(r_1-y+b)(r_3-y-b)}{(r_2-y+b)(r_4-y-b)} \ , \tag{14a}$$

$$\frac{\partial I}{\partial y} = - \log \frac{(r_1-x+a)(r_3-x-a)}{(r_4-x+a)(r_2-x-a)} \ , \tag{14b}$$

$$\frac{\partial I}{\partial z} = - \tan^{-1} \frac{(a-x)(b-y)}{zr_1} - \tan^{-1} \frac{(a+x)(b-y)}{zr_2} - \tan^{-1} \frac{(a+x)(b+y)}{zr_3} - \tan^{-1} \frac{(a-x)(b+y)}{zr_4} \ , \tag{14c}$$

and,

$$r_1^2 = (a-x)^2 + (b-y)^2 + z^2 \ , \tag{15a}$$

$$r_2^2 = (a+x)^2 + (b-y)^2 + z^2 \ , \tag{15b}$$

$$r_3^2 = (a+x)^2 + (b+y)^2 + z^2 \ , \tag{15c}$$

$$r_4^2 = (a-x)^2 + (b+y)^2 + z^2 \ . \tag{15d}$$

An extension of the half-space technique requires a new harmonic function, $\Phi^*(x,y,z)$, the introduction of a stress-free plane parallel

to the displacement discontinuity at a distance h, and a new set of boundary conditions:

$$\Delta\omega=-t \ , \ |x|\leq a \ , \ |y|\leq b; \quad z=-h, \tag{16a}$$

$$\Delta\omega=0 \ , \ \text{elsewhere} \ ; \quad z=-h, \tag{16b}$$

$$\sigma_z = \tau_{xz} = \tau_{yz} = 0 \ ; \quad z=0. \tag{16c}$$

$\Phi^*(x,y,z)$ is derived by Berry and Sales (1962) and is:

$$\Phi^*(x,y,z)=-\frac{2}{\alpha_1-\alpha_2}(\alpha_1\Phi(x,y,z-h_1)-\alpha_2\Phi(x,y,z-h_2)) \ , \tag{17}$$

where,

$$h_j = h/\alpha_j \ , \qquad j=1,2. \tag{18}$$

This, then, requires a change in the values of ϕ_1 and ϕ_2:

$$\phi_1 = \frac{\alpha_1}{1+q_1}(\Phi(x,y,z_1+h_1)+\Phi(x,y,z_1-h_1) - \frac{2}{\alpha_1-\alpha_2}(\alpha_1\Phi(x,y,z_1-h_1)-\alpha_2\Phi(x,y,z_1-h_2))) \ , \tag{19a}$$

$$\phi_2 = \frac{\alpha_2}{1+q_2}(\Phi(x,y,z_2+h_2)+\Phi(x,y,z_2-h_2) - \frac{2}{\alpha_1-\alpha_2}(\alpha_1\Phi(x,y,z_2-h_1)-\alpha_2\Phi(x,y,z_2-h_2))) \ . \tag{19b}$$

Therefore, (19) and (13)-(15) represent the solution to the problem whose boundary conditions satisfy (16).

Finally, the surface displacements (on the z=0 plane) above the displacement discontinuity can be solved by using (6), (8), (9), (13)-(15) and (19). The solutions are lengthy, and involve constants needed for the solutions of the displacement field.

First, depending on the values of the elastic moduli used in (8), α_j can be either real or complex conjugates. To assure surface displacements that are always real, a set of new constants, K_1 and K_2, are introduced; whereby,

$$k_1 = (1-\nu_1^2)^{1/2} ((E_1/E_2)-\nu_2^2)^{-1/2} , \tag{20a}$$

$$k_2 = ((E_1/2\mu) - \nu_2(1+\nu_1))((E_1/E_2) - \nu_2^2)^{-1} . \tag{20b}$$

Here, ν_1 and ν_2 are the ratio $-\varepsilon_x/\varepsilon_y$ and $-\varepsilon_z/\varepsilon_y$, respectively. μ is the shear modulus (rigidity) defined in the vertical plane. Thus, two cases can evolve depending on the values of α_j. If α_1 and α_2 are positive or complex conjugates, K_1 is always positive; and when they are real, $K_2 > K_1$. If α_1 and α_2 are complex, then $-K_1 < K_2 < K_1$.

Second, the geometric constants are defined as:

$$X_1^2 = \frac{(a-x)(b-y)}{h^2} , \tag{21a}$$

$$X_2^2 = \frac{(a+x)(b-y)}{h^2} , \tag{21b}$$

$$X_3^2 = \frac{(a+x)(b+y)}{h^2} , \tag{21c}$$

$$X_4^2 = \frac{(a-x)(b+y)}{h^2} , \tag{21d}$$

and,

$$Y_1^2 = \frac{(a-x)^2+(b-y)^2}{h^2} \quad , \tag{22a}$$

$$Y_2^2 = \frac{(a+x)^2+(b-y)^2}{h^2} \quad , \tag{22b}$$

$$Y_3^2 = \frac{(a+x)^2+(b+y)^2}{h^2} \quad , \tag{22c}$$

$$Y_4^2 = \frac{(a-x)^2+(b+y)^2}{h^2} \quad . \tag{22d}$$

Third, two recurring constants are given:

$$A_n = Y_n^2 + (k_2/k_1)^2 \quad , \qquad n=1,2,3,4 \quad , \tag{23a}$$

$$B_n = (A_n^2+(k_1^2-k_2^2)/k_1^4)^{1/2} \quad , \quad n=1,2,3,4 \quad . \tag{23b}$$

The displacement field for Case I ($0 < K_1 < K_2$) is given by:

$$u_o(x,y) = \frac{k_1 t}{2^{1/2}\pi(k_2-k_1)^{1/2}} \{\log \frac{(D_1-C_1+2(b-y)/h)(D_2+C_2+2(b-y)/h)}{(D_1+C_1+2(b-y)/h)(D_2-C_2+2(b-y)/h)}$$

$$+ \log \frac{(D_3-C_3+2(b+y)/h)(D_4+C_4+2(b+y)/h)}{(D_3+C_3+2(b+y)/h)(D_4-C_4+2(b+y)/h)}\} \quad , \tag{24}$$

$$v_o(x,y) = \frac{k_1 t}{2^{1/2}\pi(k_2-k_1)^{1/2}} \{\log \frac{(D_1-C_1+2(a-x)/h)(D_2+C_2+2(a-x)/h)}{(D_1+C_1+2(a-x)/h)(D_2-C_2+2(a-x)/h)}$$

$$+ \log \frac{(D_3-C_3+2(a+x)/h)(D_4+C_4+2(a+x)/h)}{(D_3+C_3+2(a+x)/h)(D_4-C_4+2(a+x)/h)}\} \quad , \tag{25}$$

$$\omega_o(x,y) = -\frac{t}{4\pi}\left\{\left(\frac{k_1+k_2}{k_2-k_1}\right)^{1/2}\sum_{n=1}^{4}\left(\tan^{-1}\frac{C_n X_n^{\,2}}{B_n+k_1 X_n^{\,4}} + \sum_{n=1}^{4}\tan^{-1}\frac{D_n X_n^{\,2}}{B_n-k_1 X_n^{\,4}}\right)\right\}, \quad (26)$$

where,

$$C_n = 2^{1/2}(k_2 A_n - k_1 B_n + (k_2/k_1)^2 - 1)^{1/2}, \quad n=1,2,3,4, \quad (27a)$$

$$D_n = (4k_1 B_n + C_n^{\,2})^{1/2}, \quad n=1,2,3,4. \quad (27b)$$

The displacement field for Case II ($-K_1 < K_2 < K_1$) is given by:

$$u_o(x,y) = -\frac{k_1 t}{2^{1/2}\pi(k_1-k_2)^{1/2}}\left\{\tan^{-1}\frac{C_1'}{D_1'+2(b-y)/h} - \tan^{-1}\frac{C_2'}{D_2'+2(b-y)/h} + \tan^{-1}\frac{C_3'}{D_3'+2(b+y)/h} - \tan^{-1}\frac{C_4'}{D_4'+2(b+y)/h}\right\}, \quad (28)$$

$$v_o(x,y) = -\frac{k_1 t}{2^{1/2}\pi(k_1-k_2)^{1/2}}\left\{\tan^{-1}\frac{C_1'}{D_1'+2(a-x)/h} - \tan^{-1}\frac{C_2'}{D_2'+2(a+x)/h} + \tan^{-1}\frac{C_3'}{D_3'+2(a+x)/h} - \tan^{-1}\frac{C_4'}{D_4'+2(a-x)/h}\right\}, \quad (29)$$

$$\omega_o(x,y) = -\frac{t}{4\pi}\left\{\frac{1}{2}\left(\frac{k_1+k_2}{k_1-k_2}\right)^{1/2}\sum_{n=1}^{4}\left(\log\frac{B_n+C_n' X_n^{\,2}+k_1 X_n^{\,4}}{B_n-C_n' X_n^{\,2}+k_1 X_n^{\,4}} + \sum\tan^{-1}\frac{D_n' X_n^{\,2}}{B_n-k_1 X_n^{\,4}}\right)\right\}, \quad (30)$$

where,

$$C'_n = 2^{1/2}(k_1 B_n - k_2 A_n + 1 - (k_1^2/k_2^2))^{1/2}, \quad n=1,2,3,4, \tag{31a}$$

$$D'_n = (4k_1 B_n - C'^2_n)^{1/2}, \quad n=1,2,3,4. \tag{31b}$$

Several comments should be made regarding the implementation of the subsidence model. First, Berry (1964) emphasizes that the theoretical displacement values should represent a maximum. Conversely, if a situation arises where the displacement values are known, the depth (h) is known and two of the three geometric parameters (a,b,t) are also known, then the theoretical value of the third parameter must represent a minimum; since, as a, b or t increases, the displacement values increase. Likewise, if h were the unknown parameter, then the theoretical h that gives the best fit must be a maximum; since displacement values decrease with increasing h and constant a, b and t.

Second, if a, b, t and h are known (or are set at constant values) then the displacement values will vary as a function of the elastic modulae (or α_1 and α_2).

Finally, the equations shows that two explicit, linear relationships exist whenever different $\omega(0,0,0)$ are calculated. First, let b be a function of a such that:

$$b = \lambda a, \tag{32}$$

where λ is a real constant. Then, for x=0, y=0, (21) and (22) respectively become:

$$X = X_1^2 = X_2^2 = X_3^2 = X_4^2 = \lambda(a^2/h^2) \tag{33}$$

$$Y = Y_1^2 = Y_2^2 = Y_3^2 = Y_4^2 = (1+\lambda)(a^2/h^2) \tag{34}$$

Consequently, (23) becomes:

$$A = A_1 = A_2 = A_3 = A_4 = Y^2+(k_2/k_1)^{1/2}\ , \tag{35a}$$

$$B = B_1 = B_2 = B_3 = B_4 = (A^2+ \frac{k_1^2-k_2^2}{k_1^2})^{1/2}\ . \tag{35b}$$

This procedure, in turn, changes (31) to:

$$C' = C_1' = C_2' = C_3' = C_4' = 2^{1/2}(k_1B-k_2A+1-(k_2^2/k_1^2))^{1/2}, \tag{36a}$$

$$D' = D_1' = D_2' = D_3' = D_4' = (4k_1B-C'^2)^{1/2}. \tag{36b}$$

Now, by substituting (33)-(36) into (30) and by letting β equal the bracketed (constant) value from (30) divided 4π, then:

$$\omega_o(0,0) = -t\beta. \tag{37}$$

By keeping a and h constant (a_c, h_c), (37) can be written as:

$$\omega_{(0,0,0)}(a_c,h_c,\alpha t) = \alpha^*\omega_{(0,0,0)}(a_c,h_c,t), \tag{38}$$

where α is any real constant.

The second explicit relationship can be seen by noting that the geometric constants, X and Y, in (33) and (34) will remain unchanged provided a and h are multiplied by the same constant, say γ. Then, for constant t (t_c):

$$\omega_{(0,0,0)}(a,h,t_c) = \omega_{(0,0,0)}(\gamma a,\gamma h,t_c) \ . \qquad (39)$$

The reliability of this type of solution has been verified by Berry (1964), for a mined coal seam of known dimensions with known surface displacements produced by the collapse of the overburden (Berry and Sales, 1961; Berry, 1963). A second test of the model vertical displacement components with respect to observed components for a subsidence event is provided in Appendix AI.

V. SUBSIDENCE MECHANICS OF PIT CRATERS

Applying subsidence mechanics to solve for the conditions necessary for pit crater formation requires the assumption that the diameter of a pit crater, when it initially formed, is of the same order as the distance between points of maximum tension (D) generated by a void at depth. If this is the case, then sets of rectilinear void parameters can be obtained that describe the dimensions of the void into which the crater collapsed.

It is advantageous to restrict as many of the subsidence variables as possible. The values of the elastic moduli used in the model are taken from Ryan (1979) and are:

$E_1 = 6.054 * 10^{11}$ dynes-cm^{-2};
$E_2 = 4.23 * 10^{11}$ dynes-cm^{-2};
$\mu = 3.5 * 10^{11}$ dynes-cm^{-2};
$\nu_1 = 0.20$;
$\nu_2 = 0.22$.

By using the information obtained from the flow unit thickness and the subvertical joint spacing in analyses of strata exposed in the wall of Devil's Throat, the model void half-width, a, can be restricted to be a multiple of the average joint spacing (approximately 1.25 m) and the model void thickness can be made a multiple of the average flow unit thickness (approximately 1.25 m). An initial void aspect ratio of 0.75 was assigned. The depth of burial, h, for the void was initially set to a range of 0.5 km to 1.5 km as suggested by seismic activity in this portion of the rift zone.

Initial trials using the parameters above have shown that the depth

of burial is the parameter upon which D is most dependent and that the assigned depth range was an order of magnitude too large. The initial trials have also shown that the value of D was independent of the void thickness (Figure 11) and that as the half-width increased by a discrete amount, the distance between points of maximum tension also increased by the same amount. Thus, if the void that is accomodating collapsed material from a pit crater is initially small and at a constant depth, then any change in the thickness of the void and small changes in the half-width of the void would not greatly effect the D value of the initial crater.

Subsequent trials at attaining meaningful D values, then, required the adjustment of the subsidence parameters. The depth of burial was reset to a range of 100 m to 500 m, a depth at which some intrusive events are believed to terminate (A. Okamura, Hawaiian Volcano Observatory, unpublished data). The half-width of the model void ranged from 5 m to 20 m - multiples of the average joint spacing. A half-width of 5 m produced a cavity width of 10 m - approximately five times the largest average joint spacing (Table IV). Thus, 5 m is assumed to be the minimum allowable value of a. It is further assumed that a cavity half-width of 20 m is a maximum value for a. The thickness was allowed to range over values that did not violate the imposed boundary conditions.

The results of the subsequent trials, shown in Figure 12, support the premise that D is largely a function of the model depth of burial, h. To visualize the relationships D and h have on pit craters, it was

Figure 11. Normalized vertical displacement vs. normalized distance from the collapse cavity centerline. The two-dimensional displacement curves are generated using a constant cavity cross sectional area and depth of burial. The individual curves are for cavity thicknesses of 0.625, 1.25, 2.5 and 5.0 m. For all curves, the points of greatest tangency occur at the same distance from the origin. These points define the areas of maximum tension. The stress regime curve is qualitative and the area under compression is schematically shown. (After Obert and Duvall, 1967, Fig. 18.2.2.)

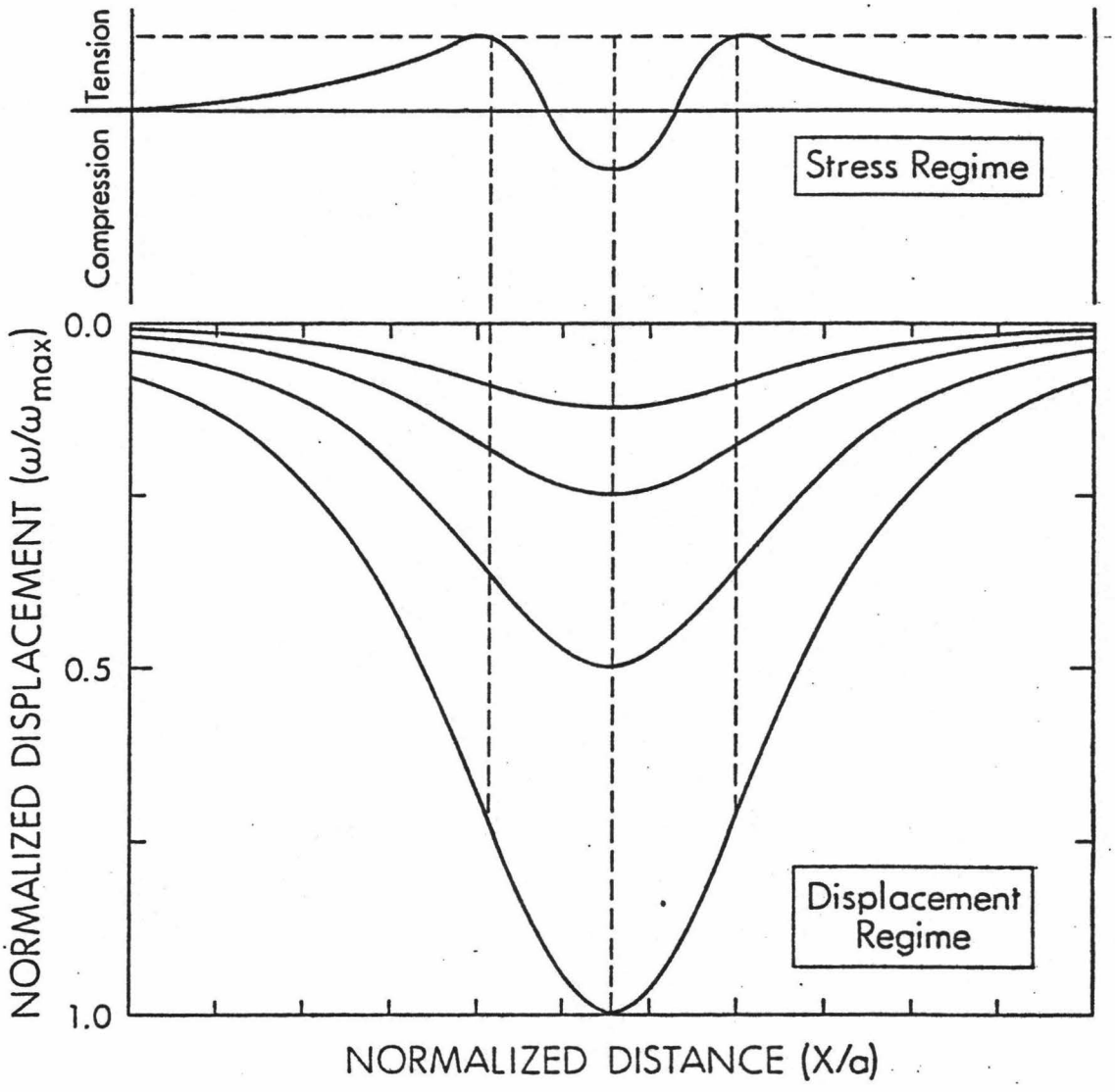
Tension
Compression
Stress Regime
0.0
0.5
1.0
NORMALIZED DISPLACEMENT (ω/ω_{max})
Displacement Regime
NORMALIZED DISTANCE (X/a)

Figure 12. Crater diameter vs. the depth of the initial cavity nucleating the collapse sequence. Model cavity depths of discrete values are used to define a zone representing the near linear relationship between cavity depth and D, the distance between points of maximum tension on the surface. The model values are generated using constant a (5 m), aspect ratio (0.75) and t (1.25 m). The error bars reflect the uncertainty in interpolating the points of maximum tension. Initial diameters from craters of Kilauea and Mauna Loa are plotted within the model generated region to yield the initial depths of burial of the voids that produced the original diameters. The observed crater depths are taken from U. S. Geological Survey topographic maps, compiled in 1963, prior to much of the lava lake activity in the region.

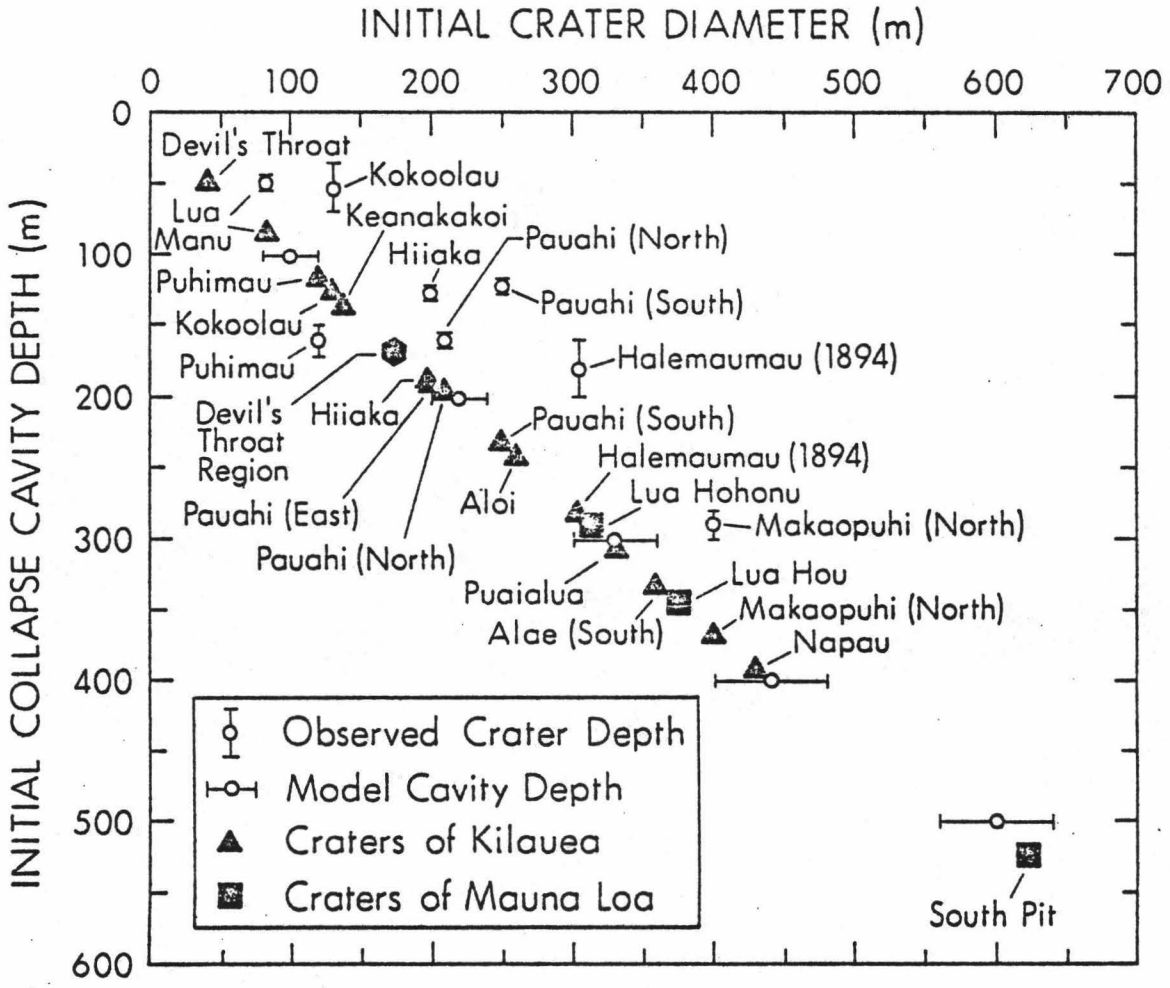
INITIAL CRATER DIAMETER (m)
0
100
200
300
400
500
600
700
INITIAL COLLAPSE CAVITY DEPTH (m)
0
100
200
300
400
500
600
Devil's Throat
Kokoolau
Keanakakoi
Lua Manu
Hiiaka
Pauahi (North)
Puhimau
Pauahi (South)
Kokoolau
Halemaumau (1894)
Puhimau
Devil's Throat Region
Hiiaka
Pauahi (South)
Halemaumau (1894)
Aloi
Lua Hohonu
Pauahi (East)
Makaopuhi (North)
Pauahi (North)
Puaialua
Lua Hou
Alae (South)
Makaopuhi (North)
Napau
Observed Crater Depth
Model Cavity Depth
Craters of Kilauea
Craters of Mauna Loa
South Pit

necessary to restore the initial pit crater diameters. These reconstructed diameters are provided in Table V. Individual pit craters in the study area have been plotted in Figure 12 using their reconstructed diameters. The resulting model depths (h) are compared with the deepest recorded depths of the pit craters, taken from the U. S. Geological Survey topographic maps that were compiled prior to much of the lava lake-forming activity, since 1963.

The values of h, taken from Figure 12, for individual craters, were used to generate maps of vertical displacement fields whose ellipticity and extent may have existed around each crater at the their times of formation. For the small pit crater (Lua Manu, Kokoolau, Devil's Throat) a constant half-width of 5 m and thickness of 1.25 m were assumed. For the group of large pit craters (Keanakakoi, Puhimau, Hiiaka, Pauahi North, Pauahi South) and Pauahi East a constant half-width of 15 m and thickness of 1.25 m were assumed. (Changes in the half-width from 5 m to 15 m produced changes in D which were within the limits of uncertainty associated with the present crater diameters. The maps, with superimposed outlines of the respective pit craters and their reconstructed diameters, and model void configurations, are shown in Figures 13-21. A composite sketch map of the Pauahi complex and the initial configuration of the three craters is provided in Figure 22.

The h value derived for each crater was compared with the crater's cumulative distance from Halemaumau along the east rift zone. The results are shown in Figure 23.

Table V. Reconstructed Pit Crater Diameters (I).
Pit crater within the study area.

Pit Crater	D (m)	Method of Reconstruction
Keanakakoi	140.	displacement opening of graben on NE side
Lua Manu	83.	diameter of present minor axis
Puhimau	173.	approx. minor axis
Kokoolau	90.	70% of present diameter
Devil's Throat	43.4	present diameter
Hiiaka	200.	crater center to 1973 vent
Pauahi North	210.	crater center to 1979 vent
Pauahi South	250.	crater center to ridge separating Pauahi North from Pauahi South
Pauahi East	140.	70% of present diameter

Figure 13. Model deformation map of Keanakakoi crater. The alternating striped-blank concentric bands correspond to the amounts of vertical subsidence generated by the model. The geometry of the model cavity is: width - 30 m; length - 40 m; thickness - 1.25 m. The heavy solid line represents the current crater margins. The heavy dashed circular line represents the configuration of the crater when it initially formed (see Table V for method of reconstruction).

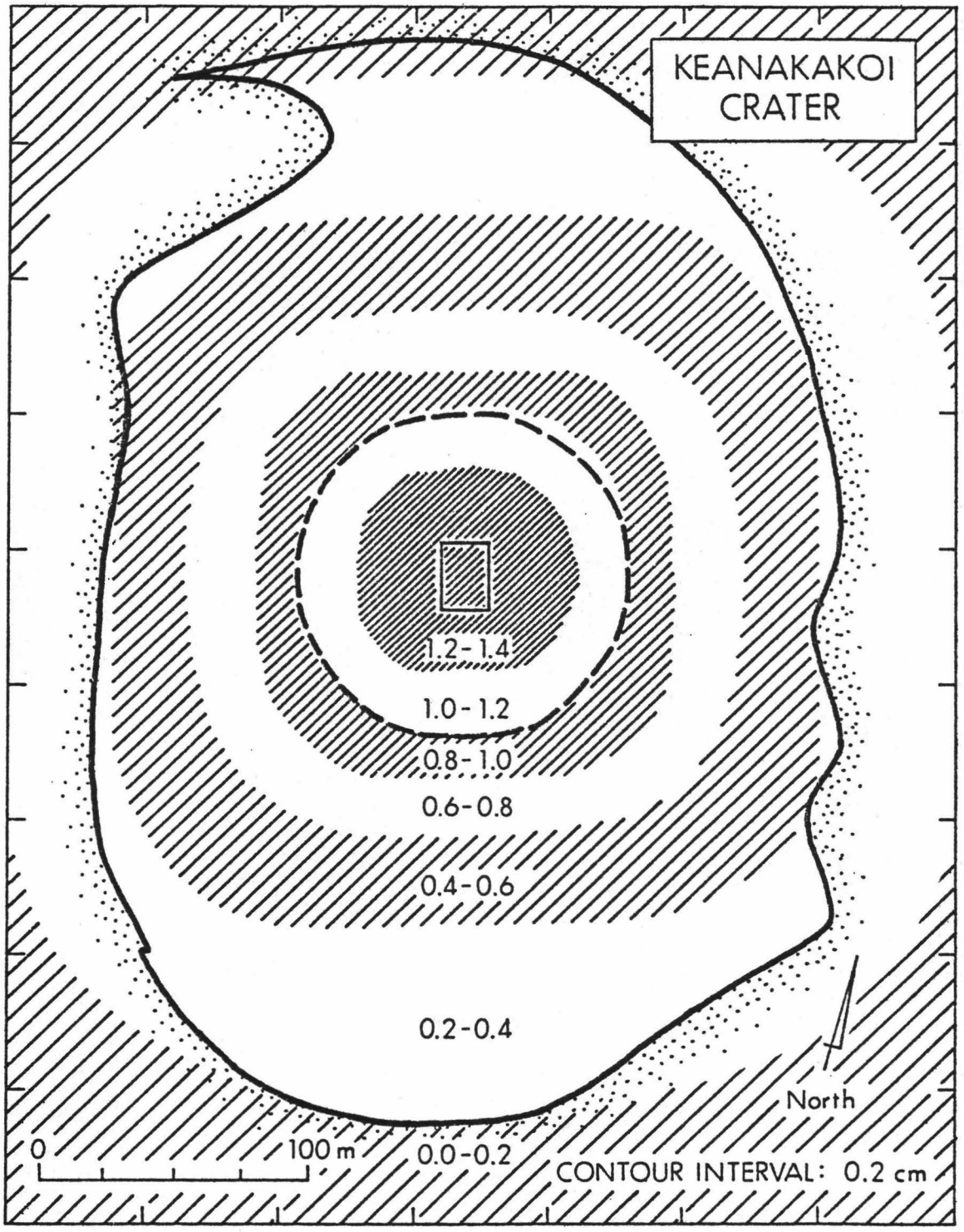
KEANAKAKOI
CRATER
1.2-1.4
1.0-1.2
0.8-1.0
0.6-0.8
0.4-0.6
0.2-0.4
0.0-0.2
North
0
100 m
CONTOUR INTERVAL: 0.2 cm

Figure 14. Model deformation map of Lua Manu crater. The alternating striped-blank concentric bands correspond to the amounts of vertical subsidence generated by the model. The subsidence values for the innermost three bands are 0.24 - 0.30 cm, 0.30 - 0.36 cm and 0.36 - 0.42 cm. The geometry of the model cavity is: width - 10 m; length - 13.3 m; thickness - 1.25 m. The heavy solid line represents the current crater margins. The heavy dashed circular line represents the configuration of the crater when it initially formed (see Table V for method of reconstruction).

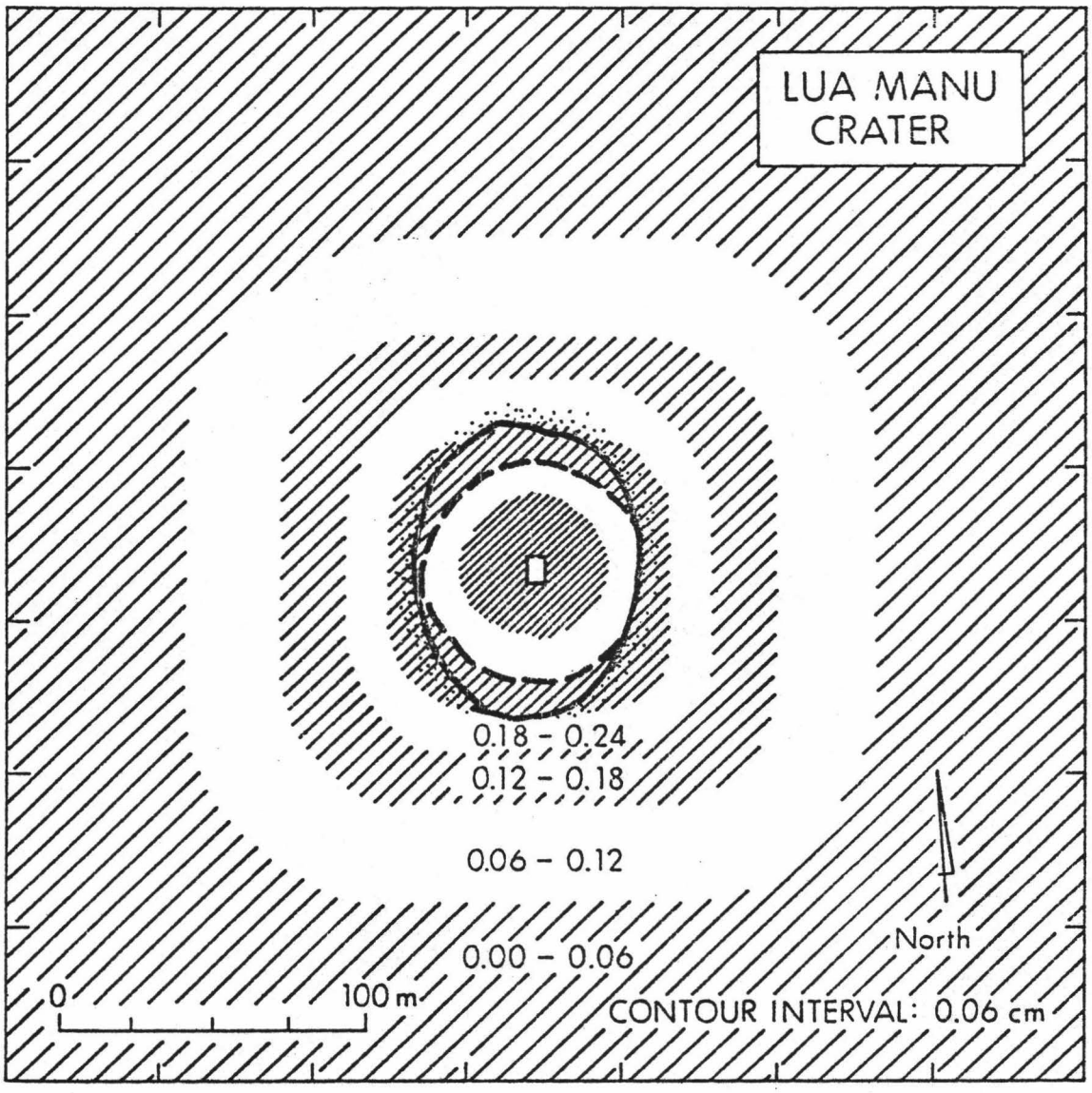
LUA MANU
CRATER
0.18 - 0.24
0.12 - 0.18
0.06 - 0.12
0.00 - 0.06
North
0
100 m
CONTOUR INTERVAL: 0.06 cm

Figure 15. Model deformation map of Puhimau crater. The alternating striped-blank concentric bands correspond to the amounts of vertical subsidence generated by the model. The geometry of the model cavity is: width - 30 m; length - 40 m; thickness - 1.25 m. The heavy solid line represents the current crater margins. The heavy dashed circular line represents the configuration of the crater when it initially formed (see Table V for method of reconstruction).

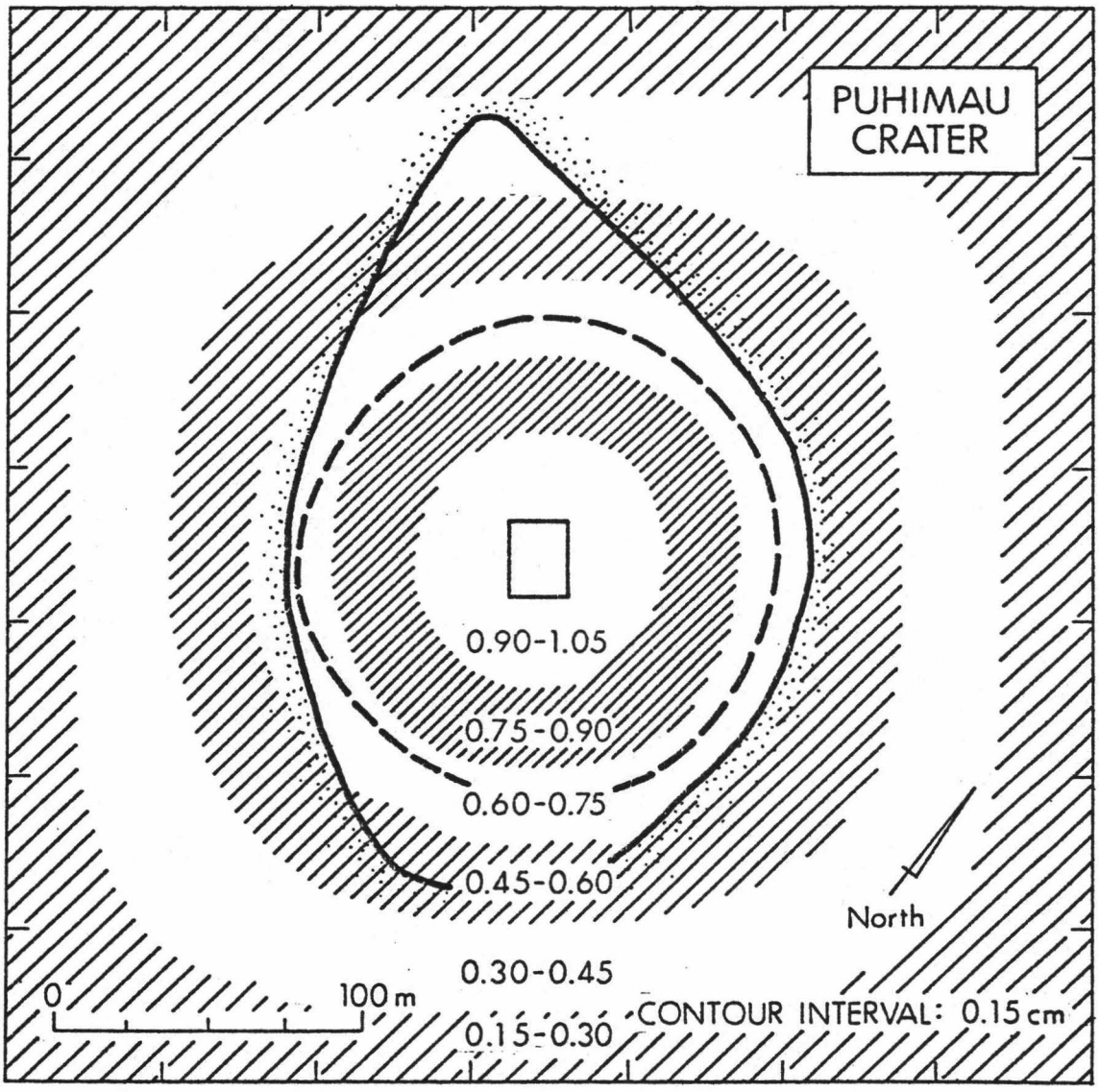
PUHIMAU
CRATER
0.90-1.05
0.75-0.90
0.60-0.75
0.45-0.60
0.30-0.45
0.15-0.30
North
0
100 m
CONTOUR INTERVAL: 0.15 cm

Figure 16. Model deformation map of Kokoolau crater. The alternating striped-blank concentric bands correspond to the amounts of vertical subsidence generated by the model. The subsidence values for the remaining bands are 0.16 - 0.20 cm, 0.20 - 0.24 cm, 0.24 - 0.28 cm, 0.28 - 0.32 cm and 0.32 - 0.36 cm. The geometry of the model cavity is: width - 10 m, length - 13.3 m, thickness - 1.25 m. The heavy solid line represents the current crater margins. The heavy dashed circular line represents the configuration of the crater when it initially formed (see Table V for method of reconstruction).

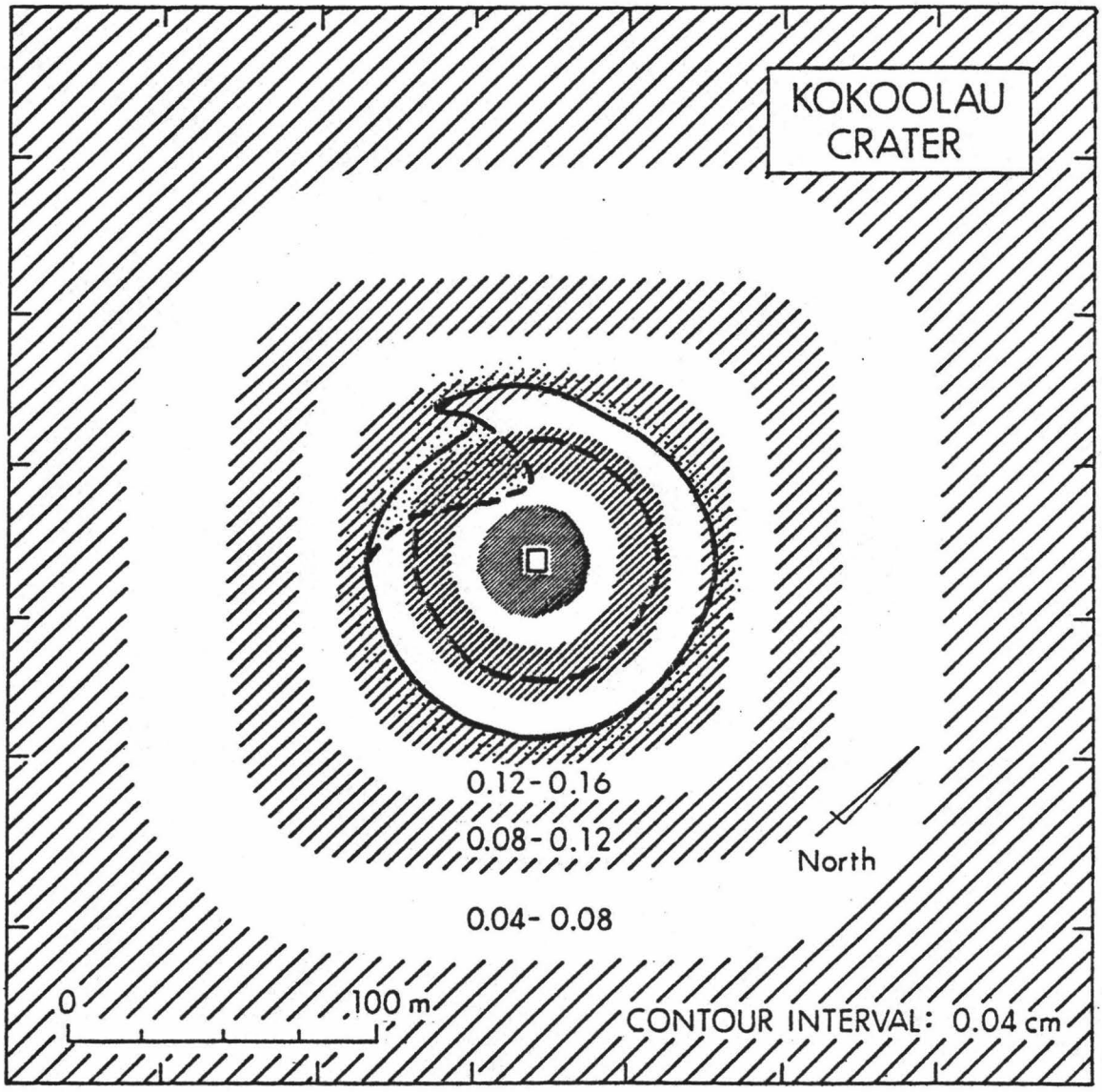
KOKOOLAU
CRATER
0.12 - 0.16
0.08 - 0.12
0.04 - 0.08
North
0
100 m
CONTOUR INTERVAL: 0.04 cm

Figure 17. Model deformation map of Devil's Throat crater. The alternating striped-blank concentric bands correspond to the amounts of vertical subsidence generated by the model. The subsidence values for the remaining bands are 0.45 - 0.60 cm, 0.60 - 0.75 cm, 0.75 - 0.90 cm, 0.90 - 1.05 cm and 1.05 - 1.20 cm. The geometry of the model cavity is: width - 10 m; length - 13.3 m; thickness - 1.25 m. The heavy solid line represents the current crater margins. The heavy dashed circular line represents the configuration of the crater when it initially formed (see Table V for method of reconstruction).

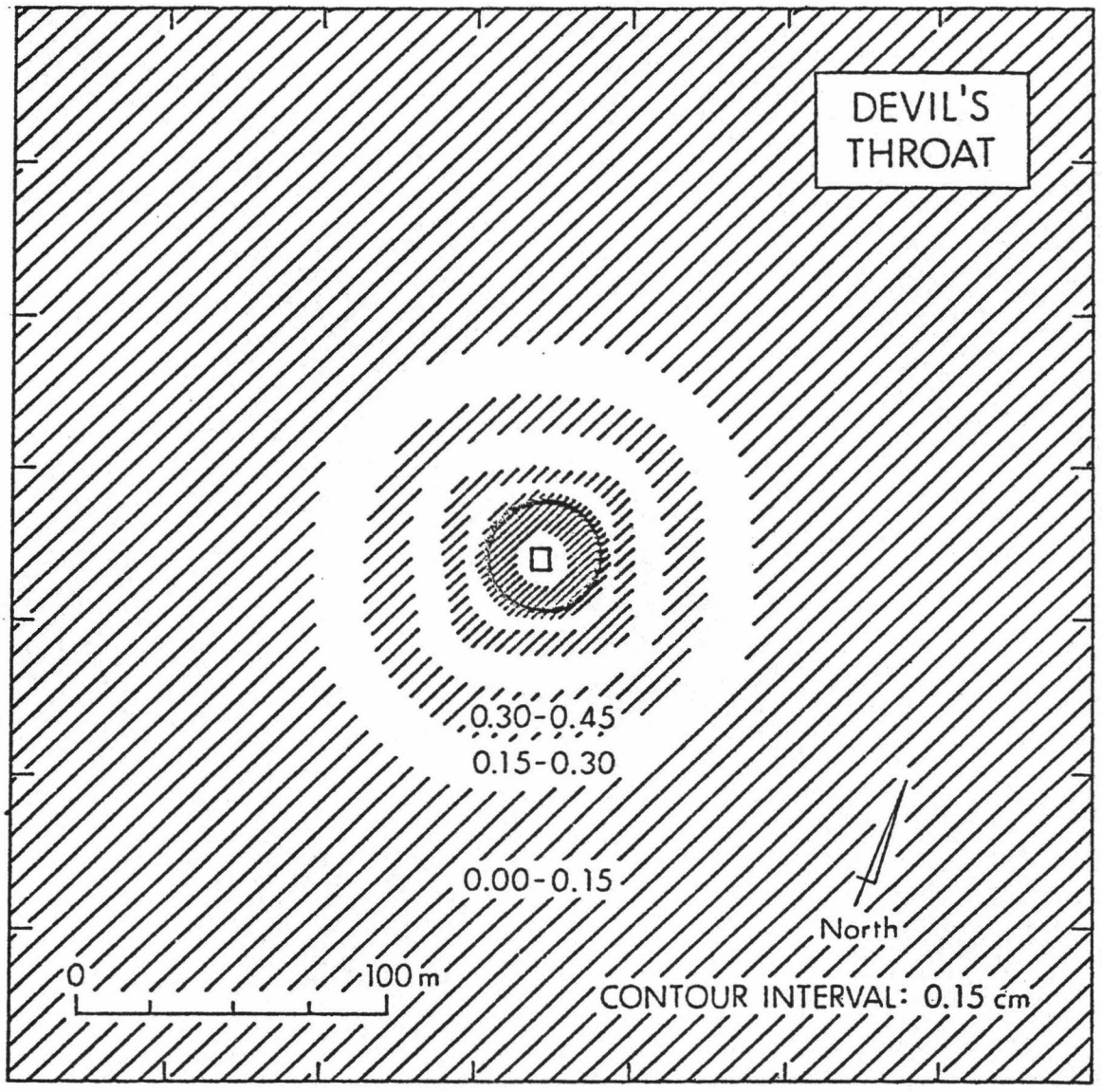
DEVIL'S
THROAT
0.30-0.45
0.15-0.30
0.00-0.15
North
0
100 m
CONTOUR INTERVAL: 0.15 cm

Figure 18. Model deformation map of Hiiaka crater. The alternating striped-blank concentric bands correspond to the amounts of vertical subsidence generated by the model. The subsidence values for the central area is 0.72 - 0.80 cm. The geometry of the model cavity is: width - 30 m; length - 40 m; thickness - 1.25 m. The heavy solid line represents the current crater margins. The heavy dashed circular line represents the configuration of the crater when it initially formed (see Table V for method of reconstruction).

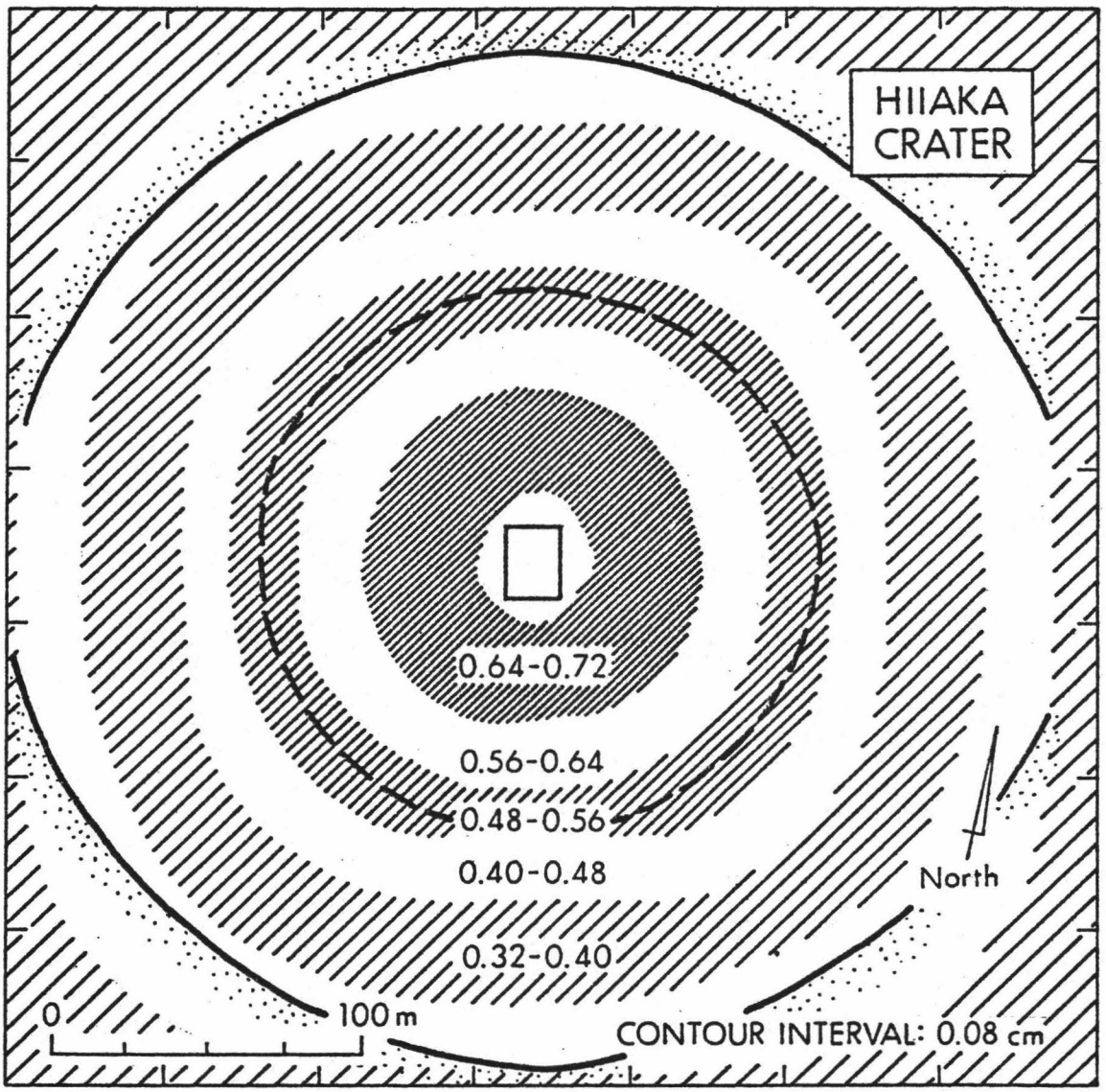
HIIAKA
CRATER
0.64-0.72
0.56-0.64
0.48-0.56
0.40-0.48
0.32-0.40
North
0
100 m
CONTOUR INTERVAL: 0.08 cm

Figure 19. Model deformation map of Pauahi North crater. The alternating striped-blank concentric bands correspond to the amounts of vertical subsidence generated by the model. The subsidence values for the central area is 0.64 - 0.72 cm. The geometry of the model cavity is: width - 30 m; length - 40 m; thickness - 1.25 m. The heavy solid line represents the current crater margins. The heavy dashed circular line represents the configuration of the crater when it initially formed (see Table V for method of reconstruction).

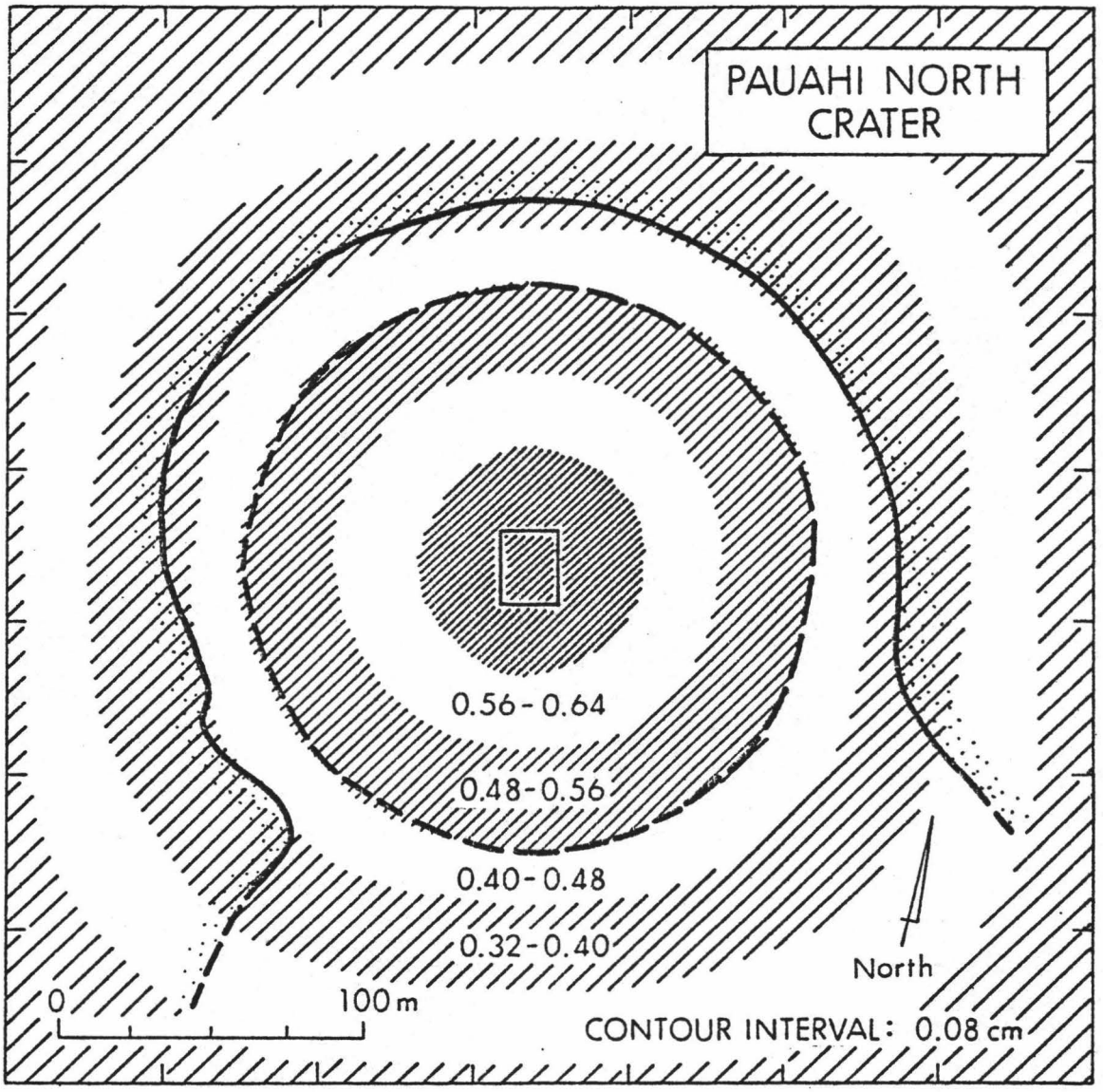
PAUAHI NORTH CRATER
0.56 - 0.64
0.48 - 0.56
0.40 - 0.48
0.32 - 0.40
North
0
100 m
CONTOUR INTERVAL: 0.08 cm

Figure 20. Model deformation map of Pauahi South crater. The alternating striped-blank concentric bands correspond to the amounts of vertical subsidence generated by the model. The geometry of the model cavity is: width - 30 m; length - 40 m; thickness - 1.25 m. The heavy solid line represents the current crater margins. The heavy dashed circular line represents the configuration of the crater when it initially formed (see Table V for method of reconstruction).

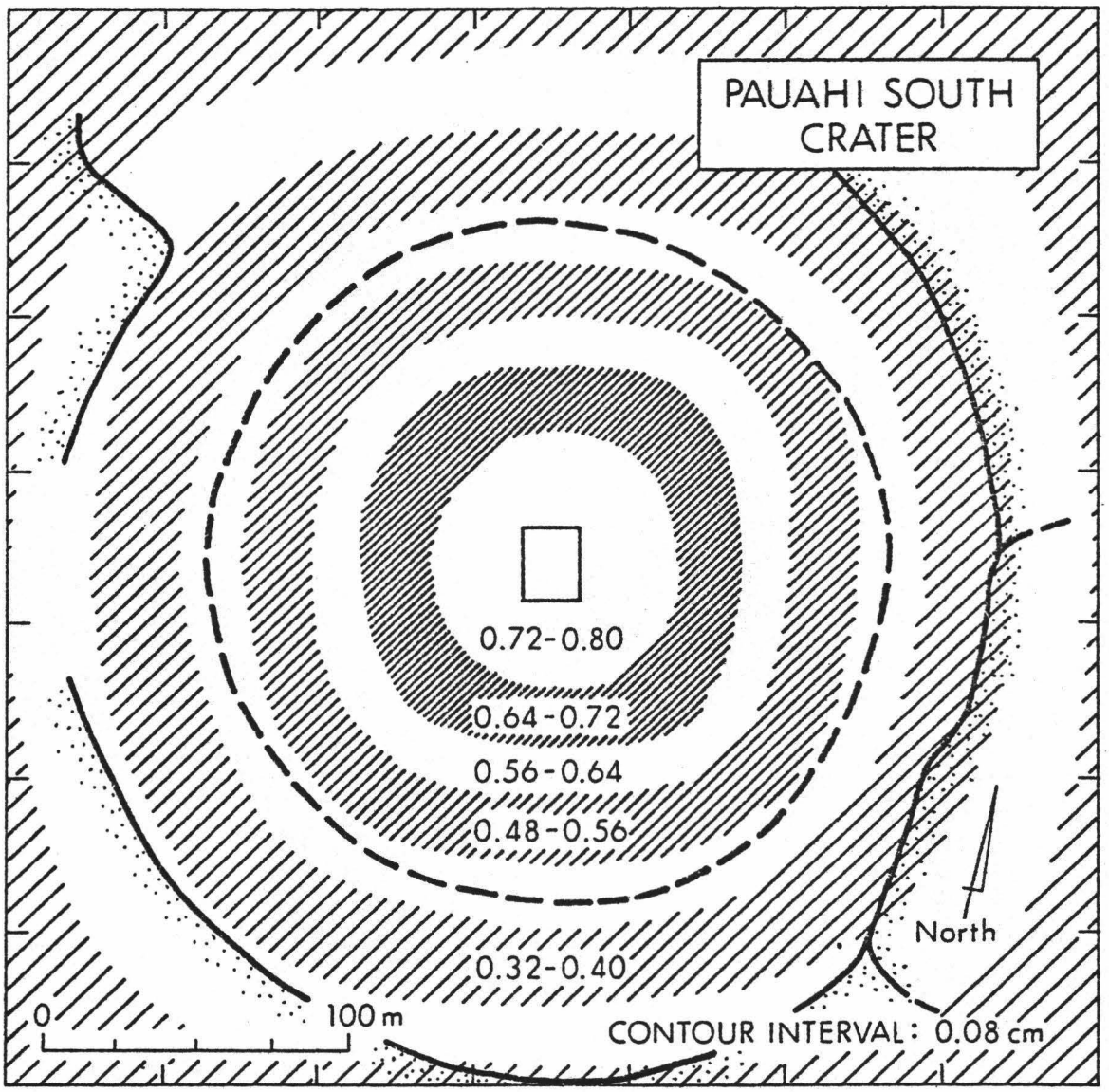
PAUAHI SOUTH
CRATER
0.72-0.80
0.64-0.72
0.56-0.64
0.48-0.56
0.32-0.40
North
0
100 m
CONTOUR INTERVAL: 0.08 cm

Figure 21. Model deformation map of Pauahi East crater. The alternating striped-blank concentric bands correspond to the amounts of vertical subsidence generated by the model. The geometry of the model cavity is: width - 30 m; length - 40 m; thickness - 1.25 m. The heavy solid line represents the current crater margins. The heavy dashed circular line represents the configuration of the crater when it initially formed (see Table V for method of reconstruction).

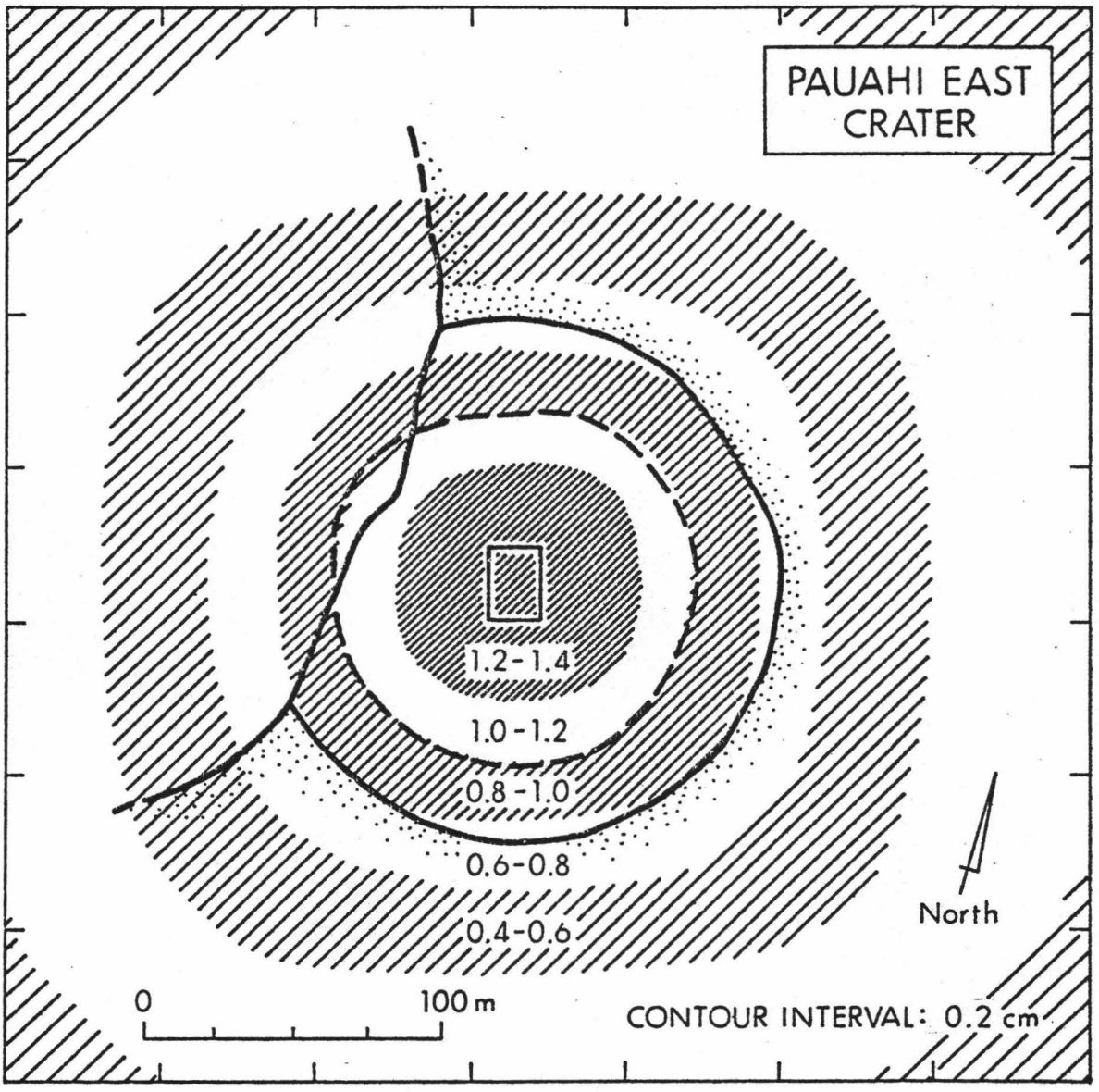
PAUAHI EAST
CRATER
1.2-1.4
1.0-1.2
0.8-1.0
0.6-0.8
0.4-0.6
North
0
100 m
CONTOUR INTERVAL: 0.2 cm

Figure 22. Sketch map of the Pauahi complex showing the relationship of the three craters' configurations when they initially formed.

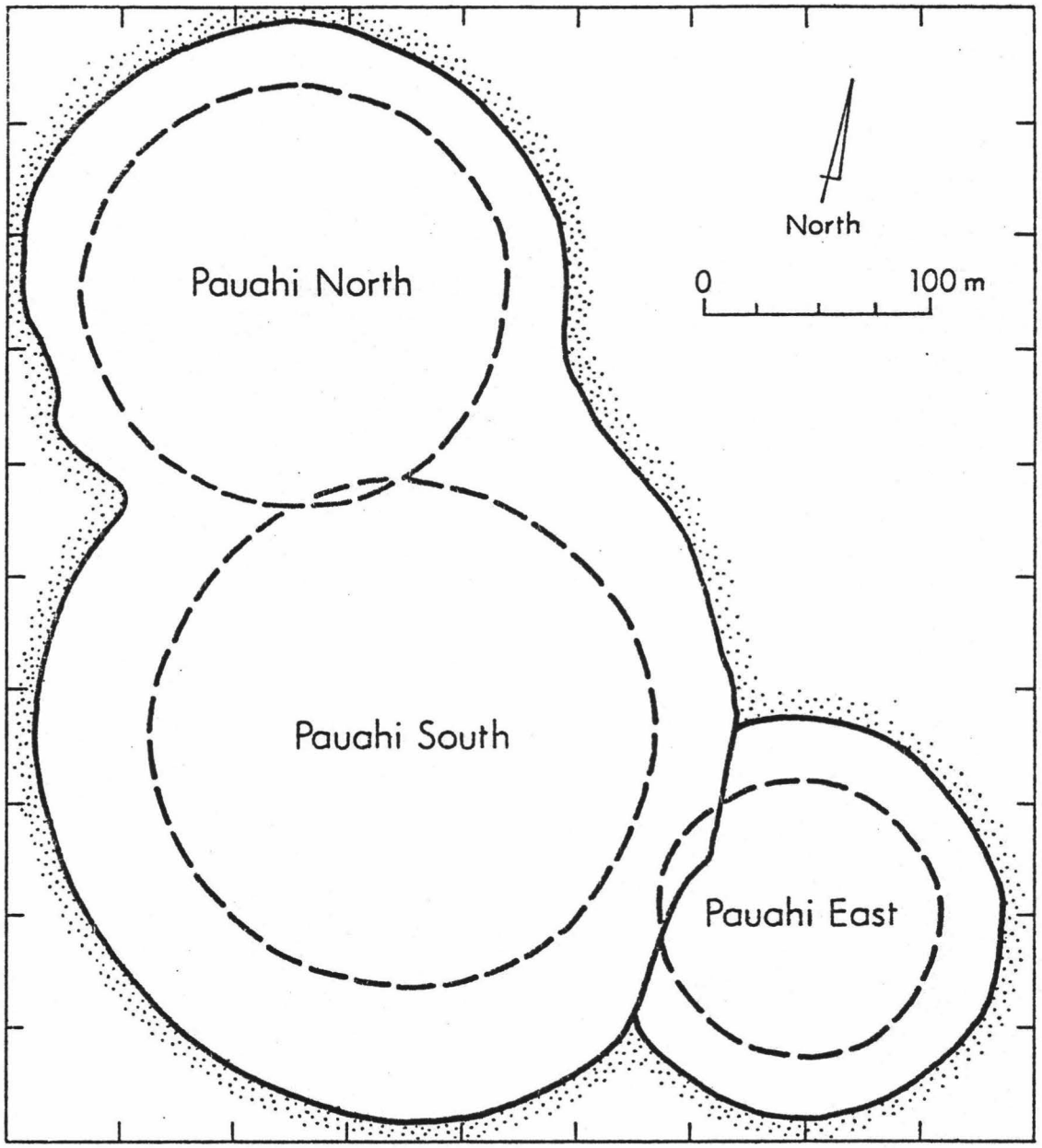
North
0
100 m
Pauahi North
Pauahi South
Pauahi East

Figure 23. The relationship between the initial collapse cavity depth and a crater's cumulative distance from Halemaumau. The pit craters' initial collapse cavities lie on a subsurface region dipping approximately 2.8°. The fit of Devil's Throat region onto this plane suggests the possibility of the region collapsing to form a much larger crater. Keanakakoi is believed to have formed partially under the influence of the summit caldera.

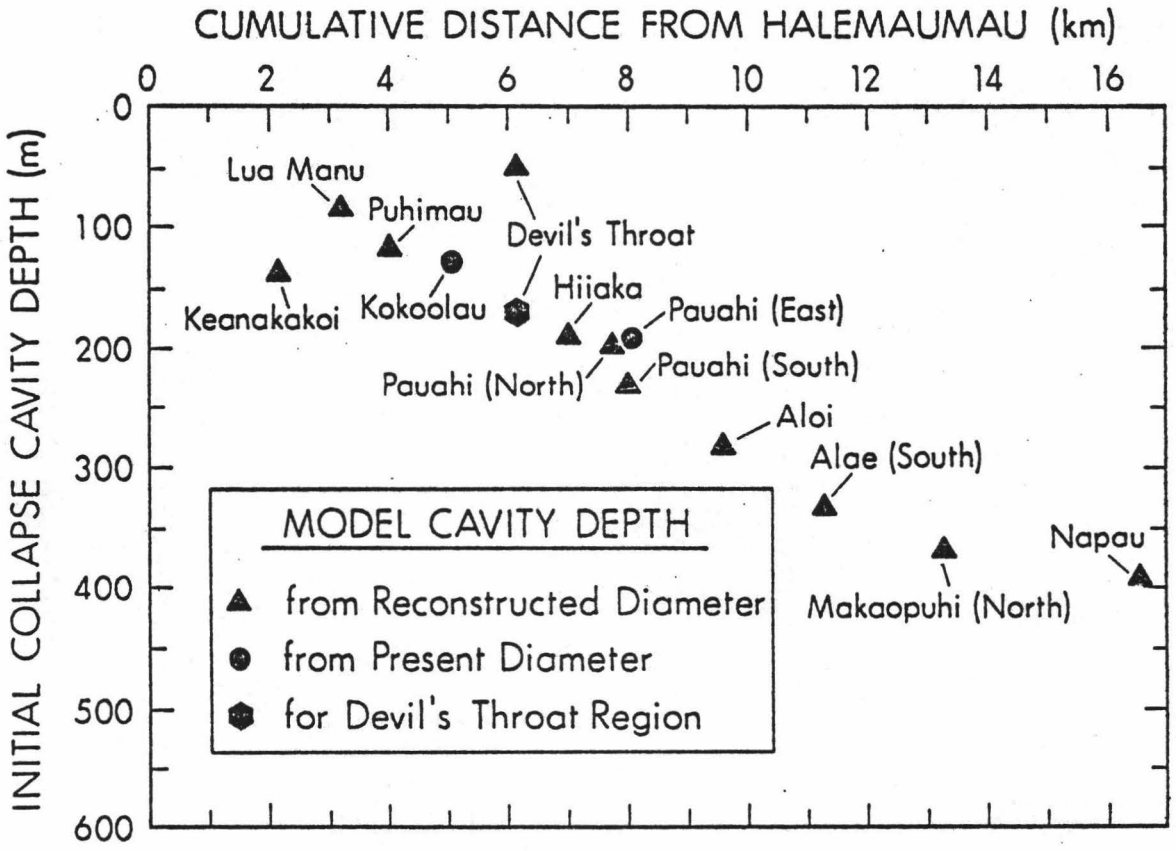
CUMULATIVE DISTANCE FROM HALEMAUMAU (km)
0
2
4
6
8
10
12
14
16
INITIAL COLLAPSE CAVITY DEPTH (m)
0
100
200
300
400
500
600
Lua Manu
Puhimau
Devil's Throat
Keanakakoi
Kokoolau
Hiiaka
Pauahi (East)
Pauahi (North)
Pauahi (South)
Aloi
Alae (South)
Napau
Makaopuhi (North)
MODEL CAVITY DEPTH
from Reconstructed Diameter
from Present Diameter
for Devil's Throat Region

DISCUSSION

An inspection of Figure 12 indicates that, in general, the model depths lie just beneath the bottom of the craters; for Devil's Throat and Puhimau, the model depths and the crater bottoms are almost coincident. This observations suggests that some craters may have current floors located immediately over the openings into which the collapsed material is falling. A second observation is the near linear relationship between the model depths and the reconstructed crater diameters.

Several additional craters beyond the study area have been added to Figure 12. From Kilauea volcano, these include Aloi, Alae (south), Makaopuhi (north), Puaialua, Napau and Halemaumau (1894 configuration). The pit craters Lua Hou, Lua Hohonu and North Pit of Mauna Loa volcano were also added. Finally, an area referred to as the Devil's Throat "region" was added. Their reconstructed depths are provided in Table VI. The h values and the distances from Halemaumau of the remaining craters in the upper east rift zone that are not part of the study area are also included in Figure 23. Examination of Figure 23 shows that most of the craters define a gently dipping planar region of 2.8^{o}. The reconstructed values of Kokoolau and Pauahi East were initially made by multiplying the present diameters by a factor of 0.7, the bulking factor for basaltic rocks (see Appendix AII). However, by using the present crater diameters the model depth values were found to coincide with the values expected from Figure 23. This has led to the supposition that Kokoolau and Pauahi East may have formed as single collapsing events

Table VI. Reconstructed Pit Crater Diameters (II).
Pit craters outside study area and
craters of Mauna Loa.

Pit Crater	D (m)	Method of Reconstruction
Devil's Throat region	173.	distance from southern bounding to fracture system 120 m to the north
Aloi	260.	crater center to April, 1970 cracks
Alae, south pit	360.	crater center to 1969 vent
Makaopuhi, north pit	400.	crater center to 1965 vent
Pualalua	330.	present diameter
Napau	430.	width of graben on NE side
Halemaumau, 1894	305.	(Macdonald and Abbott, 1977)
Lua Hou	375.	present diameter
Lua Hohonu	313.	present diameter
North Pit	625.	present diameter

along their current boundaries.

Devil's Throat appears to have formed so recently that no reconstruction of it's diameter was warranted, relative to it's position in Figure 23. However, the fact that the Devil's Throat "region" fit extremely well in Figure 23, suggests that this region may develop as a future large pit crater. It seems possible that Devil's Throat pit crater may have formed within one area of tension (Figure 11); the other area of tension being defined by the fracture system located 130 m NW of the crater.

Keanakakoi is a crater that does not fit well in the plane of depths in Figure 23. Since this crater is adjacent to the summit caldera, it is presumed that the conditions that accompanied Keanakakoi's formation were dictated largely by the close proximity to the caldera.

VI. SUMMARY DISCUSSION

The subsidence model used to describe pit crater formation mechanics requires some reiteration and expansion. The model uses the results of the flow unit thickness and the joint spacing studies as guides to determine the values of the input parameters: cavity width, 2a and thickness, t. In short, collapse of blocks into a cavity would not occur unless the cavity is of dimensions that could accomodate the blocks. A cavity half-width of 5 m appears to be the minimum value necessary to initiate and sustain collapse. The model cavity thickness of 1.25 m (also the average observed flow unit thickness) is used because it does not violate the initial model condition of $t<a$. However, the results are unchanged; Figure 11 clearly shows that a change in t does not effect D.

The observation from field studies and airphoto analyses that all the craters in the study area are bounded by N65°E-N75°E fractures leads to the conclusion that the craters are formed in tensional environments. Furthermore, these bounding faults have been manifested as fractures along which upward and lateral migration of magma can take place. The eruptive fissures that transect the craters have been interpreted as the craters' initial bounding faults.

The planar region, dipping 2.8° southeastward, upon which the craters' initial collapse cavity depths lie, may represent an older free surface of Kilauea. This surface may possibly contain an older, structural feature that, when intersected by the N65°E-N75°E fractures, provides the conditions necessary for pit crater formation.

The field observations made at Lua Manu and Puhimau describe the role of bounding faults and circumferential fractures in rotating blocks inward and their subsequent collapse. The analysis of the fractures around Devil's Throat reveal that the crack-opening-displacements increase as the distance to the crater's edge decreases.

The results of the flow unit thickness and joint spacing studies of the Devil's Throat section, combined with the observations of rotated blocks and crater wall collapse, suggest that the tensile strength of the basalt in situ is actually the amount of tensile stress needed to part a flow unit at the subvertical joint planes.

VII. CONCLUSIONS

1). A subsidence model, allowing the recovery of the three-dimensional void geometry at depth, has been applied to the pit craters of Kilauea. The model predicts initial surface deformation patterns of a similar geometry and extent to that expected to be associated with the pit craters, based on their reconstructed diameters. The deformation patterns produced by the model are nearly circular (Figures 13-21) and show high subsidence gradients that correspond with the reconstructed configurations of the craters.

2). The critical parameter in the initial subsidence mechanics of pit craters is the depth of burial, h. A change in h produces a significant change in the surface deformation pattern. Changes in the width, 2a, and the void aspect ratio, ξ, do not alter the geometry of the deformation pattern significantly. Changes of the thickness, t, produce changes in subsidence amounts but do not effect the distance between points of maximum tension, D (Figure 11).

3). The relationship between initial void depth, h, and pit crater diameter is nearly linear, based on a study of 16 Kilauean craters and 3 craters from Mauna Loa. The relationship between h and a crater's cumulative distance from Halemaumau is also nearly linear and defines a gently sloping (2.8^{o}) plane upon which lies the initial void that acts to form a pit crater.

4). Circular deformation fields, leading to circular pit craters, can

be produced by rectilinear voids at depth.

5). The evolutionary path of pit crater formation includes the mass wastage of crater walls, defined frequently by bounding faults that are oriented approximately N65°E-N75°E for the upper east rift zone. The extent of erosional activity within a pit crater can be determined, in part, by the amount of vegetation in the crater.

6). Finally, the Devil's Throat "region" also requires an initial void that lies on the 2.8° dipping plane and is an area in which a larger pit crater will probably develop.

APPENDIX AI

The application of the subsidence mechanics to broad scale deformation was accomplished by comparing model generated subsidence curves, given geologically reasonable input parameters, with curves corresponding to the observed deformation on Kilauea's summit from 4 December, 1972 to 12 May, 1973 (Hawaiian Volcano Observatory, unpublished data). The generated curve producing the best fit is shown in Figure 24. The model input parameters used are:

a = 800 m;
ξ = 0.70 (same as observed);
t = 1, 2 and 3 m;
h = 2.5 km.

The elastic moduli used are (Ryan, 1979):

$E_1 = 6.054 * 10^{11}$ dyne/cm^2;
$E_2 = 4.23 * 10^{11}$ dyne/cm^2;
$\nu_1 = 0.20$;
$\nu_2 = 0.22$;
$\mu = 3.5 * 10^{11}$ dyne/cm^2.

The approach used in recovering the best fit involved generating model subsidence curves for a large array of input parameters combinations, selecting those combinations that produced maximum subsidence values comparable to the observed maximum subsidence and isolating the combinations that exhibited subsidence attenuation on the same order as observed attenuation through normalized curves (i.e., Figure 24). Further details of the application of subsidence mechanics to the summit area of Kilauea are presented elsewhere (Ryan and others, in preparation).

Figure 24. Normalized subsidence curves corresponding to the eruptive event of May 5, 1973. The subsidence curves for intrusion thicknesses of 1, 2 and 3 m and the observed subsidence curve are normalized by the maximum vertical displacement generated by the 3 m thick intrusion. The distance is normalized by the intrusion half-width (800 m).

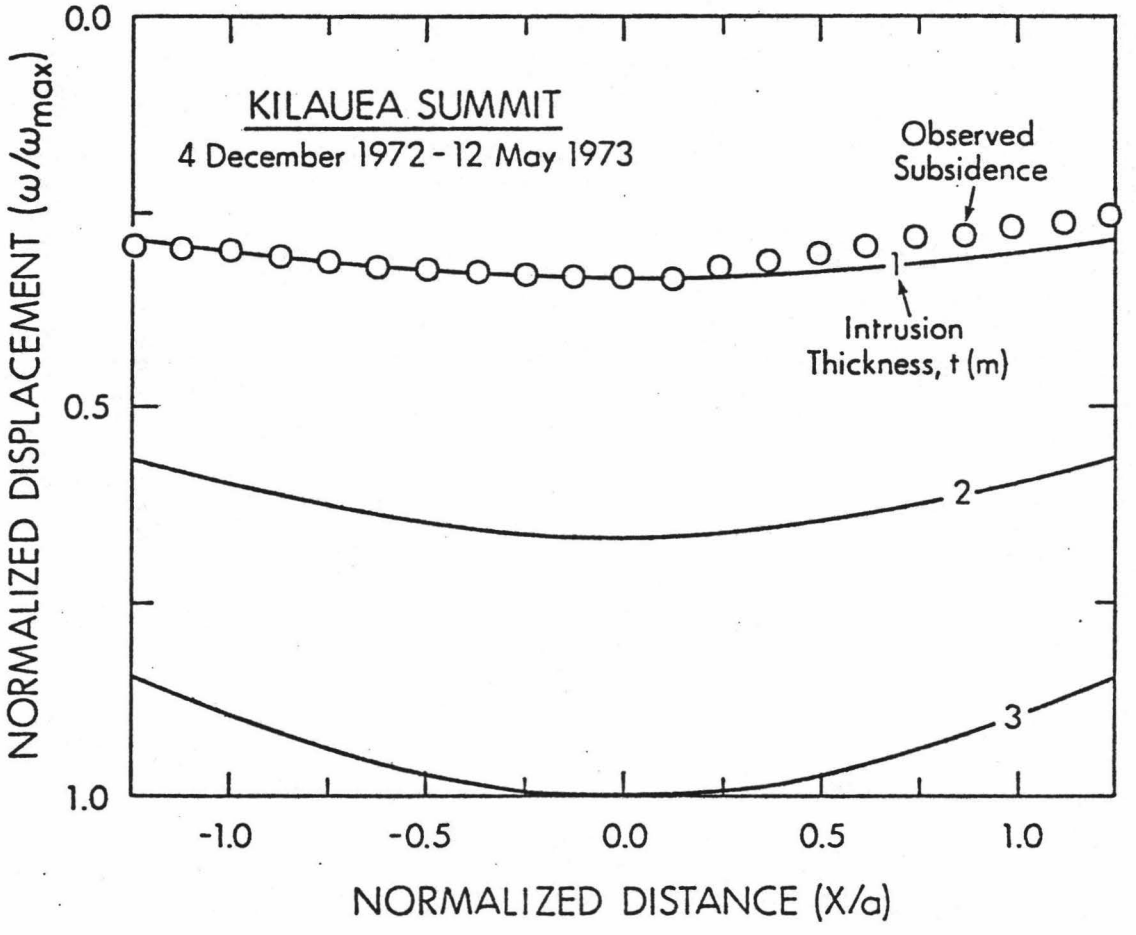
KILAUEA SUMMIT
4 December 1972 - 12 May 1973
Observed Subsidence
Intrusion Thickness, t (m)
1
2
3
0.0
0.5
1.0
-1.0
-0.5
0.0
0.5
1.0
NORMALIZED DISPLACEMENT (ω/ωmax)
NORMALIZED DISTANCE (X/a)

APPENDIX AII

Obert and Duvall (1967) suggest that the void space whose volume was initially the volume of the collapsed portion of a mine (V_t) will become progressively smaller as more interblock voids are left in the pile of caved material. If V_o is the volume of unbroken rock extracted (or caved) and allowing k to be the ratio of the volumes of broken rock to unbroken rock; then, the cave process will halt when

$$V_t = V_o(k/k-1).$$

The variable 1/k, termed here as the bulking factor, ranges from 0.67 to 0.99, depending on the packing ability of various rock types and fragment sizes. For many basalts the bulking factor is about 0.7.

BIBLIOGRAPHY

Berry, D. S., 1960, An Elastic Treatment of Ground Movement Due to Mining - I. Isotropic Ground: J. Mech. Phys. Solids, v. 8, p. 280-292.

Berry, D. S., 1963, An Elastic Treatment of Ground Movement Due to Mining - Corrigendum: J. Mech. Phys. Solids, v. 11, p. 373-375.

Berry, D. S., 1964, The Ground Considered as a Transversely Isotropic Material: J. Rock Mech. Mining Sci., v. 1, p. 159-167.

Berry, D. S. and Sales, T. W., 1961, An Elastic Treatment of Ground Movement Due to Mining - II. Transversely Isotropic Ground: J. Mech. Phys. Solids, v. 9, p. 52-62.

Berry, D. S. and Sales, T. W., 1962, An Elastic Treatment of Ground Movement Due to Mining - III. Three Dimensional Problem, Transversely Isotropic Ground: J. Mech. Phys. Solids, v. 10, p. 73-83.

Brigham, W. T., 1909, The Volcanoes of Kilauea and Mauna Loa on the Island of Hawaii: Mem. B. P. Bishop Museum, v. II, no. 4, (Kraus Reprint Co., 1974), 608 pp.

Green, A. E. and Zerna, W., 1954, Theoretical Elasticity: Oxford University Press, 457 pp.

Jackson, D. B., Swanson, D. A., Koyanagi, R. Y., and Wright, T. L., 1975, The August and October 1968 East Rift Eruptions of Kilauea Volcano, Hawaii: U. S. Geol. Survey Prof. Paper 890, 33 pp.

Jaeggar, T. A., 1947, Origin and Development of Craters: Geol. Soc. Amer. Memoir 21, 508 pp.

Macdonald, G. A. and Abbott, L., 1977, Volcanoes in the Sea: University of Hawaii Press, 441 pp.

Obert, L. and Duvall, W. I., 1967, Rock Mechanics and the Design of Structures in Rock: J. Wiley and Sons, Inc., 650 pp.

Ryan, M. P., 1979, High Temperature Mechanical Properties of Basalt: Ph. D. Thesis, The Pennsylvania State University, University Park Pennsylvania, 417 pp.

Ryan, M. P., Blevins, J. Y. K. and Okamura, A. T., (in prep.), Subsidence Mechanics of Magma Reservoirs, Kilauea Volcano, Hawaii.

Swanson, D. A., Duffield, W. A., Jackson, D. B., and Peterson, D. L., 1979, Chronological Narrative of the 1969-1971 Mauna Ulu Eruption of Kilauea Volcano, Hawaii: U. S. Geol. Survey Prof. Paper 1056, 55 pp.

Wilson, R. M., 1935, Ground Surface Movements at Kilauea Volcano, Hawaii: Univ. Hawaii Research Publications, no. 10, 56 pp.